1966

The Mössbauer effect in bismuth ferrate

Bruce A. Banks

Department:

THE MÖSSBAUER EFFECT IN BISMUTH FERRATE

BY

BRUCE A. BANKS

A

THESIS

submitted to the faculty of

THE UNIVERSITY OF MISSOURI AT ROLLA

in partial fulfillment of the requirements for the

Degree of

MASTER OF SCIENCE IN PHYSICS

Rolla, Missouri

1966

Approved by

Robert A. Gerson (advisor) R. S. Vandall

W. J. James Don C. Hopkins

ABSTRACT

The magnetic hyperfine structure of the Fe^{57} nuclei in bismuth ferrate was investigated using the Mössbauer effect. Mössbauer effect spectrometer was built with consideration given to the elimination of vibration and the optimizing of the source, absorber, and detector geometries to produce the largest fractional Mössbauer effect per fractional standard deviation. The internal magnetic field at the Fe nuclei in $BiFeO_3$ was determined to be (482 ± 9) kilooersteds at room temperature.

ACKNOWLEDGEMENT

The author wishes to express his sincere appreciation for the countless helpful suggestions offered to him by Professor Robert Gerson and William Denno. The author also wishes to thank his wife Judith Banks for her great help in the preparation of this thesis.

TABLE OF CONTENTS

LIST OF ILLUSTRATIONS

Figures Page

LIST OF TABLES

I. INTRODUCTION

The Mössbauer effect is a valuable tool for investigating the chemical and physical properties of a crystal lattice. The shape of the Mössbauer spectrum is highly dependent upon the physical and chemical properties of the crystal lattice. The Fe^{57} isotope is the most convenient isotope to study with the Mössbauer effect and is found to have a natural abundance of 2.245 % (see Table 1). Although the Fe^{57} isotope comprises only 0.4 % of the molecular weight of $BiFeO_3$, it was feasible, without resorting to Fe^{57} enriched isotopes, to use the Mössbauer effect to investigate the nature of the Fe^{57} nucleus in the perovskite lattice of $BiFeO_3$ (see Figure 1). The per cent effect was expected to be small because of the low concentration of Fe^{57} nuclei and the large electronic absorption of the gamma rays due to the remaining 99.6 % of the molecular weight. Magnetic susceptibility measurements made on $BiFeO_3$ had indicated that $BiFeO_3$ is antiferromagnetic (3). This magnetic property is detectable by the Mössbauer effect, and the strength of the internal magnetic field is measureable by Mössbauer investigation. To obtain a Mössbauer spectrum for $BiFeO_3$, it was necessary to construct a gamma ray modulation device which would be efficient, stable, linear, and distortion-free over the long periods of time necessary to obtain the required statistics to detect the small effect.

TABLE I (1, page 456)

ISOTOPES OF IRON

ISOTOPE	% NATURAL ABUNDANCE	HALF LIFE
$_{26}Fe^{52}$		7.8 hours
$_{26}Fe^{53}$		8.9 hours
$_{26}Fe^{54}$	5.90	
$_{26}Fe^{55}$		2.94 years
$_{26}Fe^{56}$	91.52	
$_{26}Fe^{57}$	2.245	
$_{26}Fe^{58}$	0.33	
$_{26}Fe^{59}$		46 days

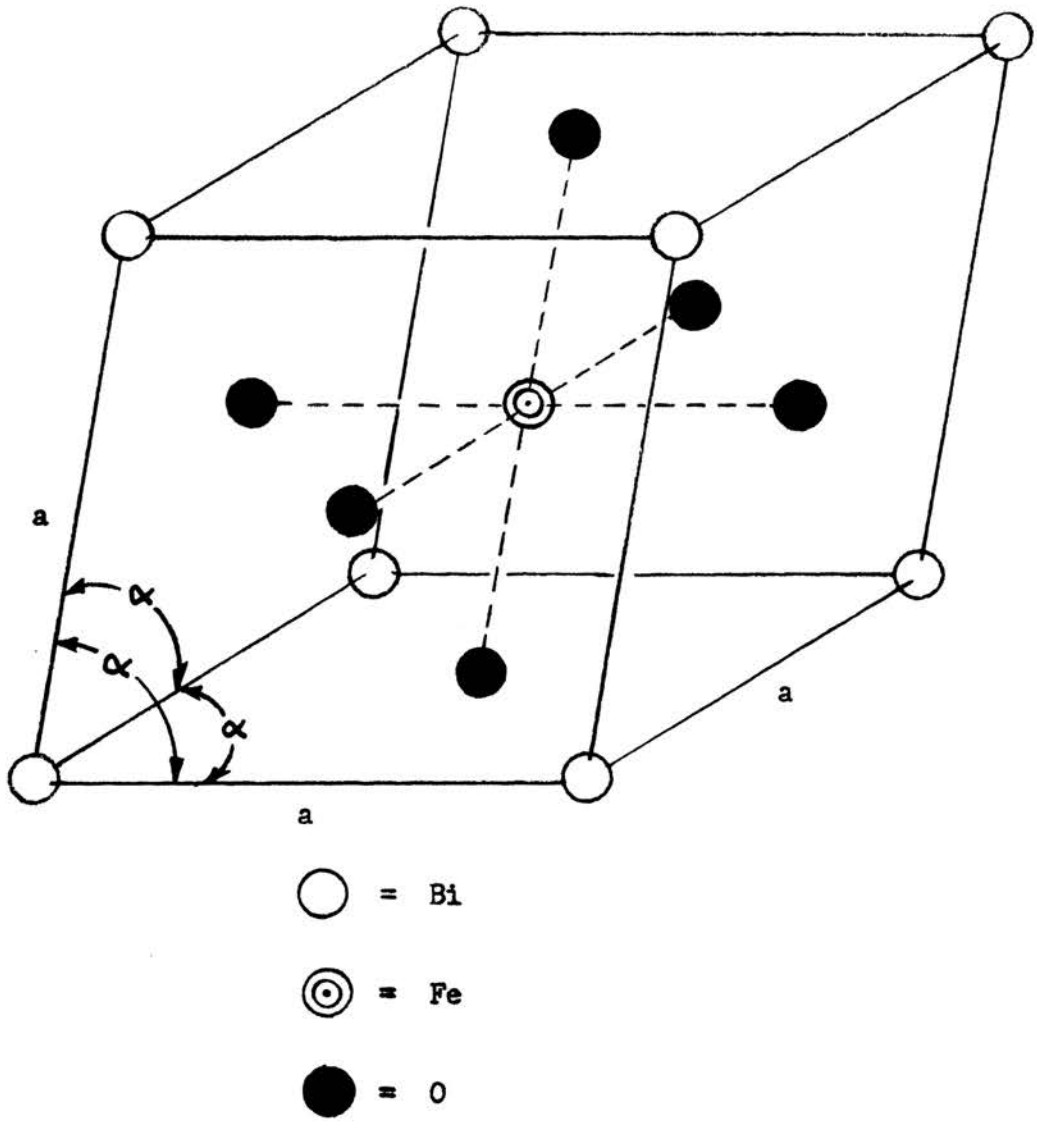

Rhombohedral distortion angle α = 89° 26.5'

Lattice parameter a = 3.951 Å (2, page 99)

Figure 1. Perovskite crystal structure of $BiFeO_3$.

II. REVIEW OF LITERATURE

A. Resonant Absorption.

The discovery of the Mössbauer effect stems from investigations of resonant processes. Acoustic resonance has been known for years and is easily demonstrated by a ringing tuning fork exciting another tuning fork of the same frequency. At the end of the nineteenth century, Lord Rayleigh suggested that similar resonant processes should occur in atomic systems (4, page 1). In 1904, R.W. Wood demonstrated that the light of the sodium D lines emitted by excited gaseous sodium atoms could be resonantly absorbed and isotropically reradiated by other sodium atoms (5). Rudolf L. Mössbauer, in 1957, discovered that resonant absorption occurred with gamma rays emitted by excited nuclei. His Nobel prize winning discovery came about through his experimental study of nuclear resonance absorption of the 129 kev gamma rays emitted by excited $_{77}Ir^{191}$ nuclei (6).

B. Gamma Ray Emission.

1. Free atom recoil.

The emission of a gamma ray from a free nucleus will cause the nucleus to recoil in the opposite direction of the gamma ray (see Figure 2). This is true from conservation of momentum.

Let M = mass of the parent nucleus.

m_o = rest mass of any general particle.

E_o = energy of the excited state of the parent nucleus.

E_γ = energy of the emitted gamma ray.

P_γ = momentum of the emitted gamma ray.

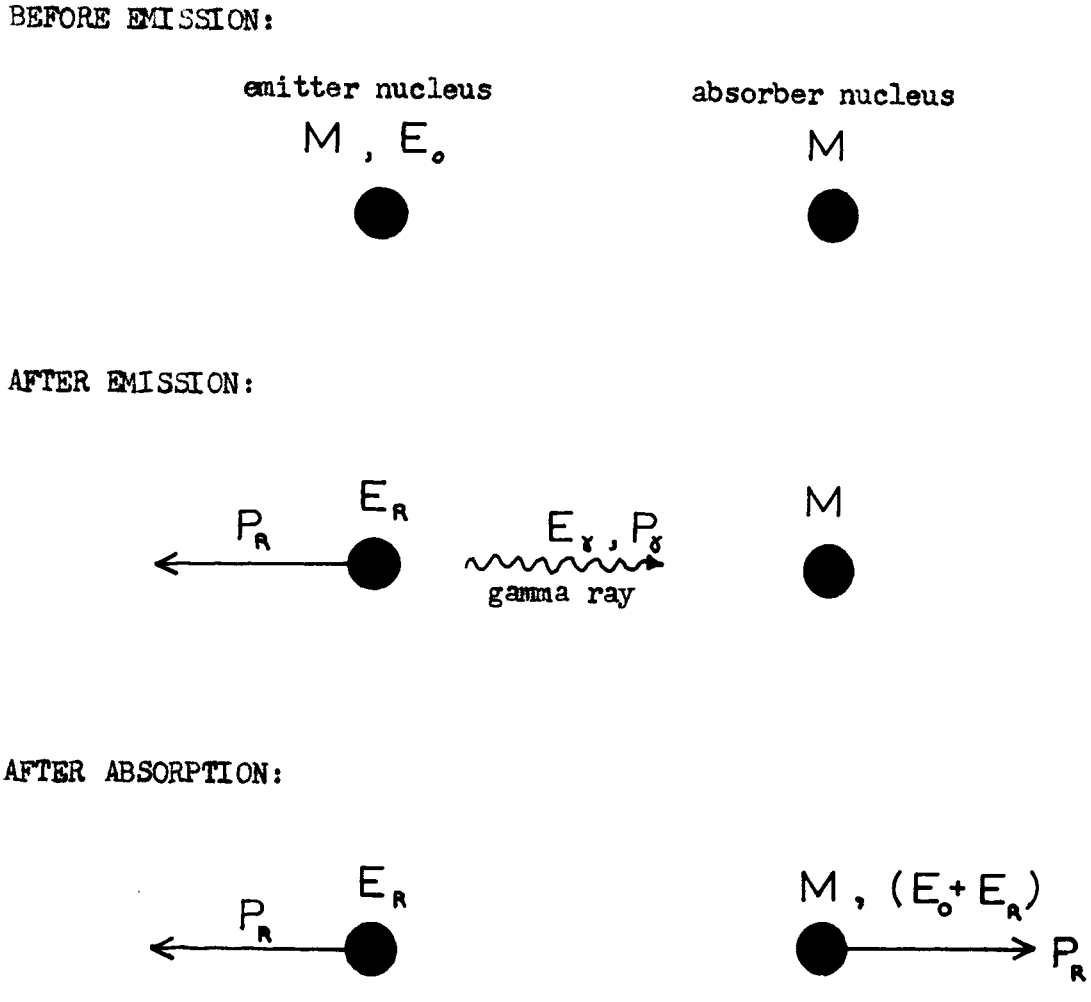

Figure 2. Free atom emission and absorption.

E_R = kinetic energy of the nucleus after emitting the gamma ray.

P_R = momentum of the nucleus after emitting the gamma ray.

In general for any particle

$$E^2 = P^2C^2 + m_o^2c^4$$

For the case of photons where $m_o = 0$,

we have $$E_\gamma = P_\gamma c .$$

Conservation of momentum yields

$$P_R = P_\gamma .$$

Thus $$Mv = \frac{E_\gamma}{C} .$$

Conservation of energy yields

$$E_o = E_R + E_\gamma$$

or $$E_o = \frac{1}{2}Mv^2 + Mvc .$$

Solving the quadratic equation for v gives

$$v = c\left[-1 \pm \left(1 + \frac{2E_o}{Mc^2}\right)^{\frac{1}{2}}\right] .$$

One chooses the + root to obtain a recoil velocity in the opposite direction from the emission of the gamma ray.

Thus $$V = C\left[-1 + \left(1 + \frac{2E_0}{Mc^2}\right)^{\frac{1}{2}}\right] .$$

The term $\frac{2E_0}{Mc^2}$ is very small, since for most experiments

$$E_0 \approx 10^4 \text{ ev}$$

and $$Mc^2 \approx 10^{10} \text{ ev} .$$

Therefore $$\frac{2E_0}{Mc^2} \approx 10^{-6} << 1$$

One can expand $\left(1 + \frac{2E_0}{Mc^2}\right)^{\frac{1}{2}}$ using the binomial expansion and neglect squared and higher powers of $\left(\frac{2E_0}{Mc^2}\right)$.

Thus $$V = \frac{E_0}{Mc} .$$

Substituting V into the formula for the recoil energy yields

$$E_R = \frac{1}{2} Mv^2 = \frac{E_0^2}{2Mc^2}$$

and $$\frac{E_R}{E_0} = \frac{E_0}{2Mc^2} \approx 10^{-6} .$$

For Fe^{57} $$E_R = 1.92 \times 10^{-3} \text{ ev}.$$

Thus the fraction of energy that is absorbed in the nuclear recoil is very small, but it is by no means insignificant when a resonant absorption is attempted. The energy spread or line width of the emitted gamma ray must be wide enough to provide an overlap with the absorption energy line width for a free atom recoil Mössbauer effect to occur. The absorbing nucleus will also receive a recoil from the incident gamma ray and will not resonantly absorb unless the gamma ray energy is within the linewidth, Γ , of the absorption spectrum. The resulting criterion for observing a Mössbauer effect from free nuclei at rest is that the linewidth is greater than or equal to twice the recoil energy.

$$\Gamma \geq 2E_R$$

This can be shown by two overlapping spectrums as in Figure 3.

2. Recoilless Emission.

Bound nuclei such as those in a crystal lattice can exhibit a finite probability to emit or absorb their characteristic gamma rays without receiving any recoil energy. This is a result of the quantization of the lattice phonon system. If we consider our lattice to behave as an Einstein solid of N atoms and 3N vibrational modes all vibrating at the Einstein frequency, ω_E , then only integral multiples of the associated phonon energy can be transferred to the lattice in the recoil process (7, page 9). Thus

$$E_R = n\hbar\omega_E \qquad \text{where} \quad n = 0, \pm 1, \pm 2, \cdots$$

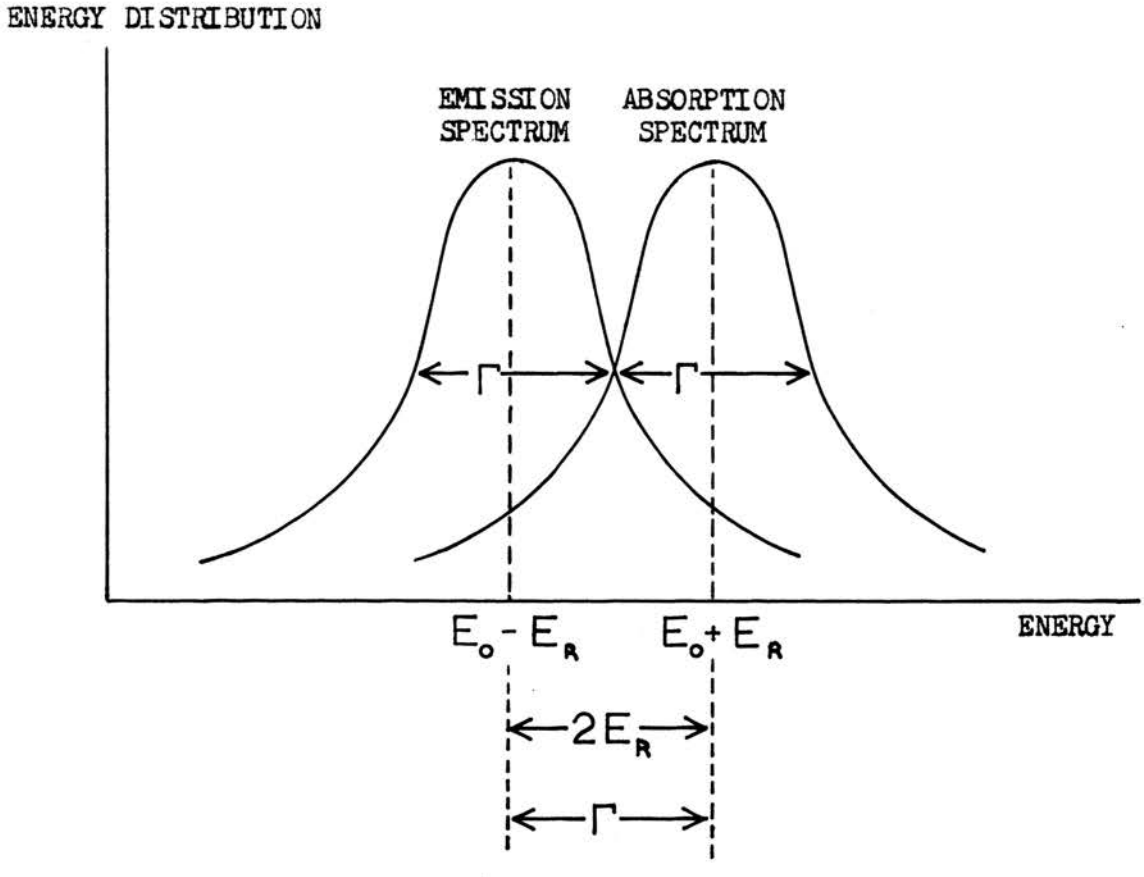

Figure 3. Free atom emission and absorption spectra.

and $\omega_E \approx 10^{13}$ radians/second for most solids.

$\hbar = \frac{h}{2\pi} =$ 1.054×10^{-27} erg sec.

The fact that n can equal zero permits the possibility of a recoilless gamma ray emission. If one averages over many emissions, the average lattice recoil energy, E_R, will be exactly that given by the free atom recoil energy (8).

$$E_R = \frac{E_o}{2Mc^2}$$

Momentum conservation requires that the lattice will receive the recoil momentum

$$P_R = \frac{E_o}{c}$$

even in the case of recoilless emission. This is not contradictory since the momentum is absorbed by the lattice as a whole, making the lattice recoil velocity very small and the recoil energy negligible, since it is proportional to the square of the recoil velocity. The crystal lattice is able to hold the emitting nucleus in place because the recoil energy is only of the order of 10^{-2} ev while the energy necessary to remove a nucleus from its lattice site is of the order of 10 ev (4, page 21). The statistical fraction of nuclei which exhibit recoilless emission is called the recoilless fraction, f. Metallic iron, represented by the Debye model with the Debye temperature, Θ_D = 400°K, yields f = 0.79 (9). The recoilless fraction is temperature dependent. The relationship is expressed in terms of the Debye-Waller factor, $2W$, for a Debye

solid (4, page 30).

$$f = e^{-2W}$$

and $$W = \frac{3E_R}{k\Theta_D}\left[\frac{1}{4} + \left(\frac{T}{\Theta_D}\right)^2 \int_0^{\frac{\Theta_D}{T}} \frac{x\,dx}{e^x - 1}\right]$$

where k = Boltzmann's constant

T = Temperature in $^{\circ}K$

The recoilless fraction for an Einstein solid at $T = 0$ is

$$f = e^{\frac{-E_R}{\hbar\omega_E}} = e^{\frac{-E_R}{k\Theta_E}}$$ (4, page 30).

Both emission and absorption lines are Lorentzian in shape (derived from the Fourier transform of a damped harmonic oscillator as the emitting nucleus) with the source and absorber full linewidths at half maxima of Γ_a and Γ_s respectively. The resulting experimentally observed linewidth is also a Lorentzian shape and of linewidth, $\Gamma_a + \Gamma_s$ (7, page 15). The Lorentzian energy dependence of the experimentally observed total cross section, σ, is given by

$$\sigma = \sigma_o \frac{1}{\left(\frac{2(E - E_o)}{(\Gamma_a + \Gamma_s)}\right)^2 + 1}$$

For Fe^{57}, $\sigma_o = 2.2 \times 10^{-18}$ cm^2, which is approximately 200 times the photoelectric absorption for the 14.37 kev gamma ray (7, page 12).

If one has an ideal Mössbauer experiment, the source and absorber linewidths are the natural linewidths given by the limit of the Heisenberg uncertainty relation.

Let ΔE = uncertainty in energy.

Δt = uncertainty in time.

τ = mean lifetime of the excited nuclear state of the emitting nucleus.

The minimum product of ΔE and Δt is

$$\Delta E \, \Delta t = \hbar$$

but $$\Delta E = \Gamma_s$$

and $$\Delta t = \tau$$

Thus $$\Gamma_s \, \tau = \hbar$$

A typical value of the lifetime, such as $\tau = 10^{-7}$ seconds for the 14.37 kev gamma ray of Fe^{57}, gives

$$\Gamma_s = 4.6 \times 10^{-9} \text{ ev.}$$

If $\Gamma_s = \Gamma_a$ then

$$\frac{\Gamma_s + \Gamma_a}{E_\gamma} = 6.4 \times 10^{-13}$$

which is the minimum fractional uncertainty in the measurement of the gamma ray energy. Experiments have been performed which have closely approximated this narrow linewidth (9, page A724).

C. Gamma Ray Modulation Techniques.

1. Mechanical systems.

If the fractional linewidth of the emitted gamma ray is narrow enough, it is possible to move the source or absorber with a relative velocity large enough to provide a Doppler shift on the order of magnitude of the linewidth. This makes it possible to experimentally measure the resonant absorption line shape. Using special relativity, let us look at a gamma ray emitted from a nucleus moving with respect to some other reference frame (see Figure 4).

Let V = velocity of the primed (source) coordinate system with respect to the unprimed (absorber) system.

ϕ = angle between the velocity vector and the line between the origin of the coordinate systems.

$E_o = h\nu_o$ = energy of the gamma ray as measured in the reference frame of the emitting nucleus.

ν_o = frequency of the emitted gamma ray as measured in the reference frame of the emitting nucleus.

$E = h\nu$ = energy of the gamma ray as measured from absorbing reference frame.

ν = frequency of the gamma ray as measured from the absorbing reference frame.

Γ = natural linewidth of source and absorber.

c = velocity of light.

From special relativity

$$\nu = \nu_o \frac{\left(1 + \frac{V}{c}\cos\phi\right)}{\sqrt{1-\left(\frac{V}{c}\right)^2}} \quad ,$$

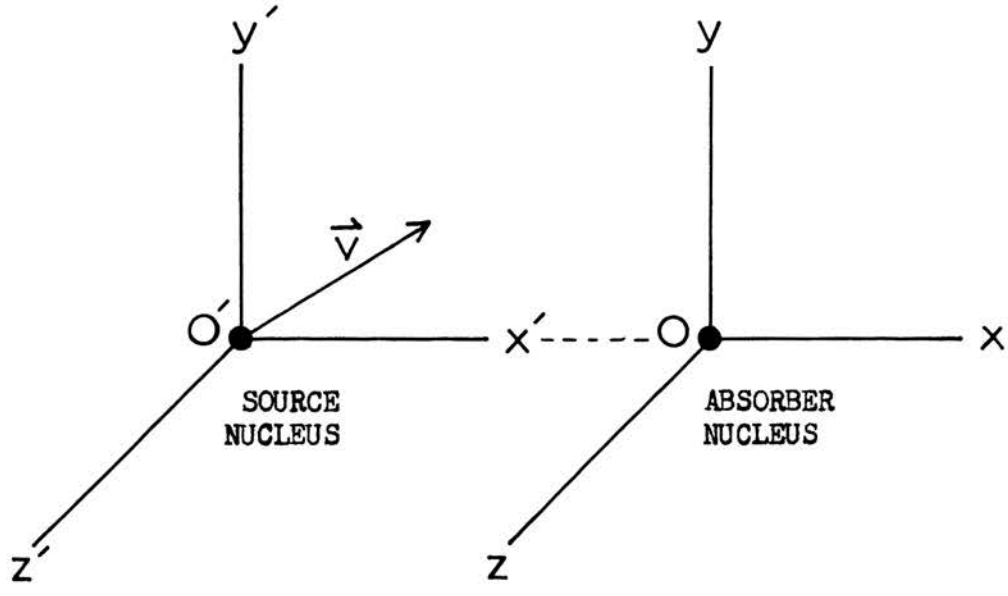

Figure 4. Source and absorber reference frames.

and $$\nu = \frac{E}{c} \quad , \quad \nu_0 = \frac{E_0}{c} \quad .$$

If one expands using the binomial expansion, the resulting expression is

$$E = E_0 \left(1 + \frac{V}{c} \cos\phi\right)\left(1 + \frac{1}{2}\left(\frac{V}{c}\right)^2 + \cdots\right) .$$

For most laboratory experiments $\frac{V}{c} << 1$, and the first order relativistic Doppler shift or red shift for $\phi = 0$ is

$$E = E_0 \left(1 + \frac{V}{c}\right) \quad .$$

To experimentally observe the absorption line shape one must be able to produce a velocity, V, such that

$$E - E_0 = \Gamma$$

therefore $$E_0 \left(\frac{V}{c}\right) = \Gamma$$

and $$V = \frac{\Gamma c}{E_0} \cong .1 \text{ mm/sec} \quad \text{for} \quad Fe^{57} .$$

This is, indeed, a conveniently slow velocity, and yet it is enough to produce the required Doppler shift. Many types of mechanical devices exist which move either the emitting source or absorbing nuclei relative to the other (see Figure 5). The proper choice of drive mechanism depends largely upon the velocities necessary for the required Doppler shift. Mechanical vibrations must be avoided in the design of a mechanical drive system, since any

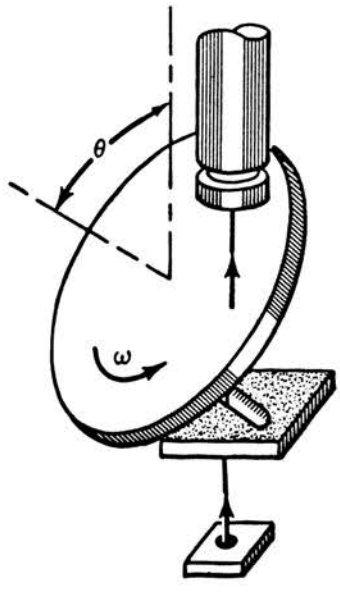

ROTATING DISK (10)

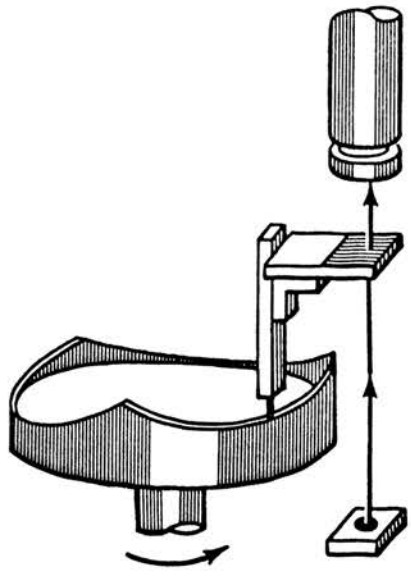

THREE-STEP CAM (10)

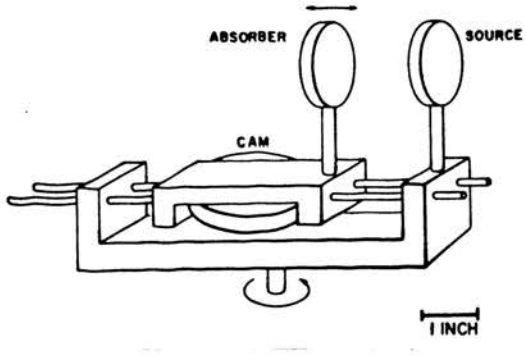

CONSTANT-VELOCITY CAM (12)

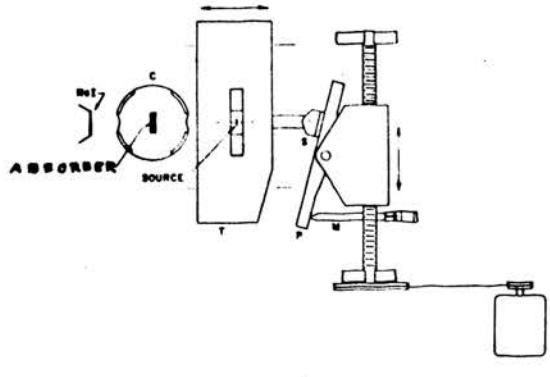

INCLINED PLANE (14)

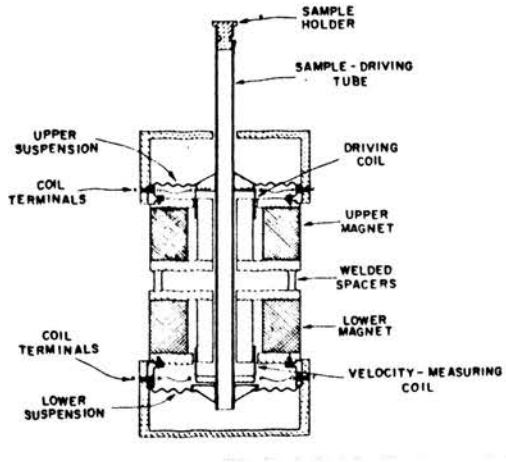

DOUBLE SPEAKER (13)

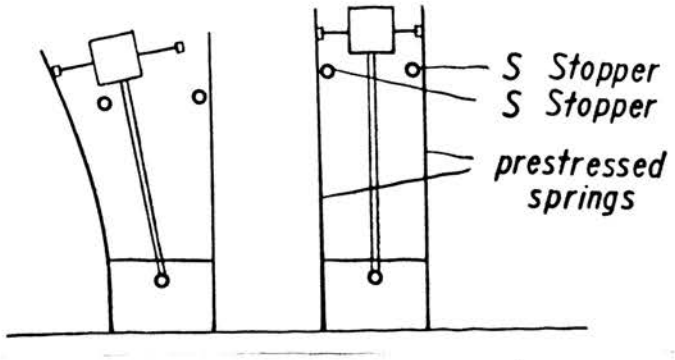

INVERTED PENDULUM (11)

Figure 5. Mechanical drive systems.

vibrational velocity will modulate the gamma ray energy. This is particularly important when the fractional linewidth, $\frac{\Gamma}{E}$, is small, such as $3.2X10^{-13}$ for the 14.37 kev gamma ray of Fe^{57} or $5.3X10^{-16}$ for the very narrow 71 kev gamma ray of Zn^{67}.

The emitting nuclei are usually diffused into a host lattice, such as a thin metallic foil disk. If the source is to move relative to the laboratory frame, it is mounted on the mechanical drive mechanism, which is capable of imparting a known relative velocity between the source and absorber.

The absorber is usually a thin slab or sheet of material containing the absorbing nuclei. One measures the count rate of the gamma rays as a function of the relative velocity between the source and the absorber. This can be done by measuring the count rate of the isotropically scattered gamma rays or measuring the reduction in count rate (due to the isotropic emission of the resonantly absorbed gamma rays) of the gamma rays passing through the absorber. The transmission measurement technique is most commonly used, because nonresonant scattering greatly reduces the magnitude of the resonance peaks in the scattered gamma ray measurement technique. The gamma rays are usually detected by means of a scintillation counter or proportional counter, depending on the energy of the gamma ray.

2. Thermal shift.

The vibrational motion of atoms in a crystal lattice will also modulate the frequency of the emitted gamma ray. The Debye cutoff frequency, ω_D, for most solids is of the order of 10^{13} radians/second, while the halflife of a typical excited state

is 10^{-9} seconds (for the first excited state of Fe^{57}). The 10^5 lattice vibrations per halflife will average the first order part of the Doppler shift to zero. Thus

$$\langle E \rangle = \langle E_0 \left(1 + \frac{v}{c} \cos\phi\right)\left(1 + \frac{1}{2}\left(\frac{v}{c}\right)^2 + \cdots\right) \rangle$$

and $$\left\langle \frac{v}{c} \cos\phi \right\rangle = 0$$

yielding $$\left\langle \frac{E - E_0}{E_0} \right\rangle \cong \frac{1}{2c^2} \langle v^2 \rangle$$

where $$\langle v^2 \rangle > 0 \quad .$$

This is a second order Doppler shift and is proportional to the mean square velocity of the atoms, which is related to the specific heat of the lattice at constant pressure, C_p, by

$$\frac{1}{E} \frac{\partial E}{\partial T} = \frac{C_p}{2Mc^2}$$

providing that the lattice forces are harmonic (15, page 79). The experimentally observed temperature shift will depend on the relative temperatures of the source and absorber. This shift can also be viewed as a time dilation, where the frequency of the emitted gamma ray can be thought of as a clock in the moving coordinate system. Although the vibrational motion of the emitting nuclei do not cause a broadening in the experimentally observed linewidth, there will be sidebands or phonon wings at

sum and difference frequencies of the vibrational and gamma ray frequencies (see Figure 6). These sideband frequencies differ in energy by hundredths of an electron volt and represent Doppler shifts corresponding to hundreds of meters per second (7, page 37).

3. Gravitational shift.

One can change the energy of a photon by letting the photon travel through a gravitational potential difference or its relativistic equivalent, an acceleration. The change in energy of the photon is the work done on the equivalent mass, m_e, of the photon.

Thus $$E - E_0 = \int_{\vec{r}_1}^{\vec{r}_2} m_e \vec{a} \cdot d\vec{r}$$

where $\vec{a}$ = acceleration or gravitational acceleration,

$\vec{r}$ = distance.

$$m_e = \frac{E_0}{c^2} = \frac{h\nu_0}{c^2} \quad .$$

The small increment of energy added to a gamma ray emitted downward through a distance of 74 feet in the field of gravity, is detectable by the Mössbauer effect (16).

4. Phase modulation.

The first order Doppler shift can be written more generally as

$$\frac{E - E_0}{E_0} = \frac{V}{c} = \frac{-1}{c} \frac{d}{dt} \int_{r_{source}}^{r_{absorber}} n(r)\, dr$$

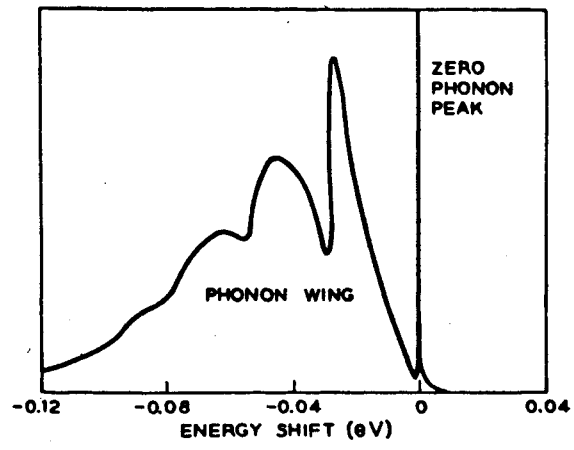

The theoretical spectrum of the 129 keV gamma ray of Ir^{191} emitted by an atom in iridium metal at low temperature. The Mössbauer spectrometer is sensitive only to the narrow, recoil-free line at zero energy shift, which contains 5.7% of the total area under the curve, (7, page 37)

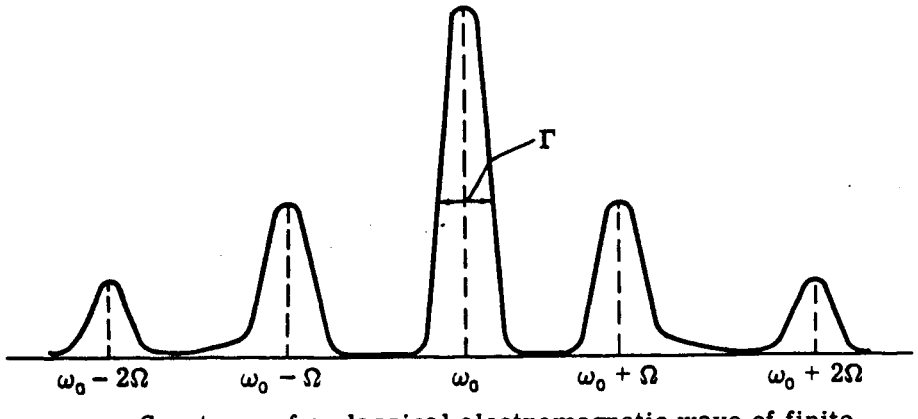

Spectrum of a classical electromagnetic wave of finite length emitted by an Einstein solid, (4, page 20).

Ω = Einstein frequency

ω_0 = Gamma ray frequency

Figure 6. Sidebands and phonon spectra.

where $n(r)$ = index of refraction (at the gamma ray frequency) of the medium between the source and absorber.

r = distance.

t = time.

The integral is the optical path length between the source and the absorber. If one had a homogeneous medium of index of refraction, n, between the source and the absorber then

$$\frac{E - E_0}{E_0} = \frac{1}{c}\left(nv - l\frac{dn}{dt}\right)$$

where $l = r_{absorber} - r_{source}$ = source to absorber distance

and $$v = -\frac{dl}{dt} \quad .$$

Thus with $v = 0$, we could modulate the phase of the waves by varying n, and obtain an energy shift. At optical frequencies, this could be achieved by varying the pressure of the air between the source and the absorber. Unfortunately at gamma ray frequencies $n-1$ is very small and the energy shift would be infinitesimal. Phase modulation can be achieved by changing the optical path length if a wedge of material with $n > 1$ is passed between the source and the absorber as in Figure 7. The energy shift will be proportional to the rate of change of wedge thickness at the point the gamma rays pass through the wedge. Using this method, the index of refraction at gamma ray frequencies has been determined for lucite and aluminum (18).

D. Isomer Shift.

An excited state nuclear wave function will be different

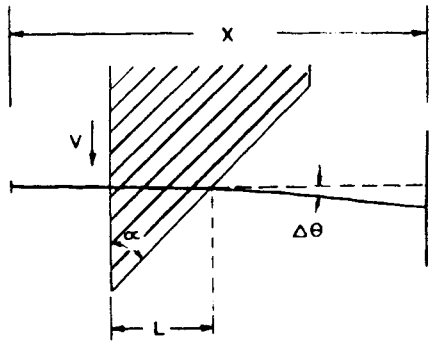

Fig. 1

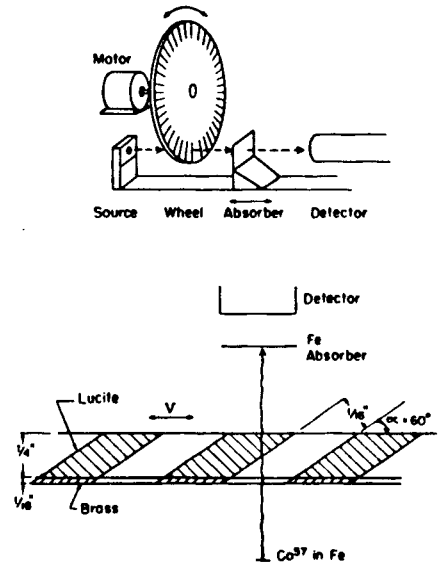

Figure 7. Phase modulation of gamma rays (18).

than the ground state wave function. Thus the effective nuclear ground state radius, R_g, and its excited state radius, R_e will also be slightly different. As a result, the nuclear electrostatic potential distributions within the nuclei will be different. The electronic wave functions will in general, overlap the nucleus giving a charge density of $-e|\Psi(0)|^2$ where $-e$ is electronic charge and $\Psi(0)$ is the net electronic wave function evaluated at the nucleus. This finite electron density at the nucleus results in a potential energy due to the nuclear electrostatic potential. This interaction potential energy is different for the ground state than for the excited state. The energy difference is given to the emitted gamma ray as the emission takes place. The source and the absorber nuclei will have the same ground and excited state radii but their electronic wave functions will be slightly different if their chemical environments are different. As a result, there is an isomer shift or energy shift in the gamma ray if the absorbing nuclei are in a different chemical environment than the source nuclei (see Figure 8). The isomer shift energy for a constant charge distribution nuclear model is:

$$\text{Isomer shift energy} = \frac{2\pi Z e^2}{5}\left(R_e^2 - R_g^2\right)\left(|\Psi_a(0)|^2 - |\Psi_s(0)|^2\right)$$

where Z = atomic number.

$\Psi_s(0)$ = net source electronic wave function evaluated at the nucleus.

$\Psi_a(0)$ = net absorber electronic wave function evaluated at the nucleus.

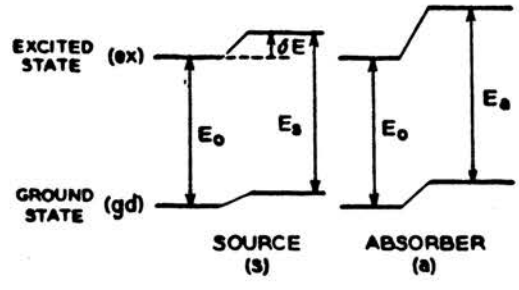

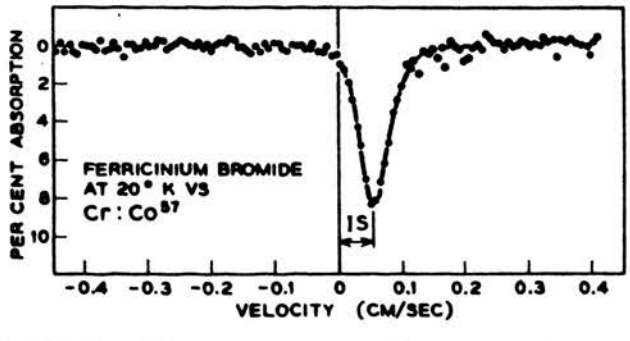

Figure 8. Isomer shift (7, page 51).

E. Quadrupole Coupling.

The nuclear electrostatic charge distribution can be written in terms of a multipole expansion. In general, the 2^n-pole moment is zero unless the nuclear spin quantum number $I \geq \frac{n}{2}$ (19, page 167). Odd order (2^{2n+1}-pole) nuclear electric multipole moments will also be zero because nuclei exhibit axial symmetry and the nuclear center of mass coincides with its center of charge. The nuclear monopole moment is simply the nuclear charge, whose interaction with the electronic wave function is responsible for the isomer shift. The nuclear dipole moment is zero, leaving the quadrupole moment as the second nonvanishing multipole term. The interaction between the nuclear quadrupole moment, $\overleftrightarrow{Q}$, and the electric field at the nucleus takes place through the electric field gradient, $\vec{\nabla}\vec{E}$, where the Hamiltonian, H, is

$$H = \overleftrightarrow{Q} \cdot \vec{\nabla}\vec{E} \quad .$$

The eigenvalues, E_Q, of H yield a splitting of all or part of the, $(2I+1)$ -fold degeneracy where

$$E_Q = \frac{Q \frac{\partial E_x}{\partial x}}{4I(2I-1)} \left[3m_I^2 - I(I+1)\right]\left[1 + \frac{\eta^2}{3}\right]^{\frac{1}{2}}$$

and $m_I = I, I-1, \cdots, -I$ = magnetic quantum number

$$\eta = \frac{\frac{\partial E_x}{\partial x} - \frac{\partial E_y}{\partial y}}{\frac{\partial E_z}{\partial z}} = \text{asymmetry parameter (7, page 61)}$$

Nuclear spins of $I = \frac{1}{2}$ remain degenerate because E_Q depends only on the square of m_I (see Figure 9). The electric field gradient at the nucleus is created by the charges on neighboring ions and the atom's own electronic wave functions. The electronic wave functions are distorted by the ionic electric field gradient and tend to amplify (antishielding) the effect of the ionic charges (7, page 61). Cubic crystal structures do not exhibit quadrupole splitting because the electric field gradient is zero.

F. Magnetic Hyperfine Structure

The interaction between the nuclear magnetic dipole moment, $\vec{\mu}$, and the internal magnetic field at the nucleus $\vec{H}_n$ (produced largely by the atom's own electrons) can be written in terms of an interaction Hamiltonian, H_m where

$$H_m = -\vec{\mu} \cdot \vec{H}_n = -g \vec{\mu}_n \cdot \vec{H}_n$$

and g = gyromagnetic ratio

μ = nuclear magneton (7, page 72)

The corresponding eigenvalues of energy are given by

$$E_m = -\mu H_n \frac{m_I}{I} = -g \mu_n H m_I$$

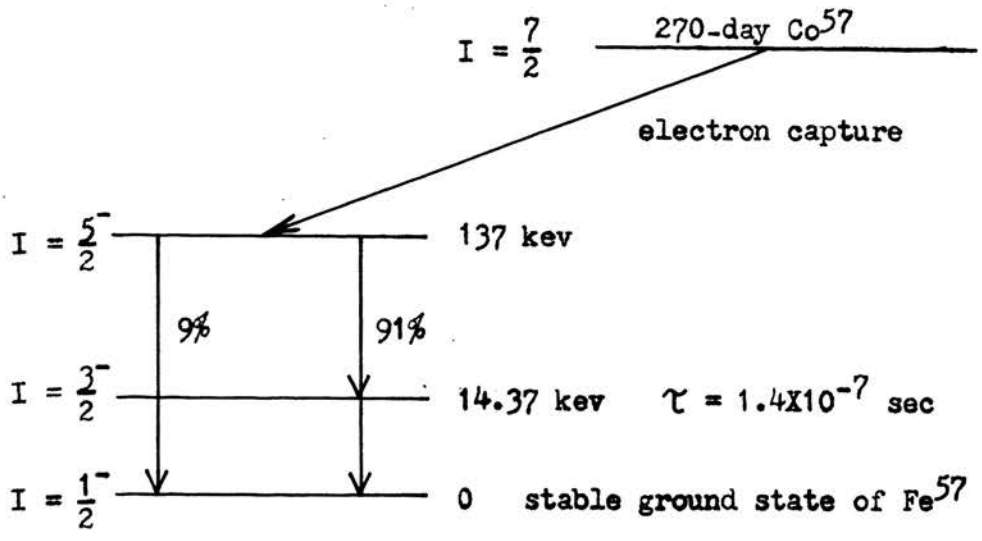

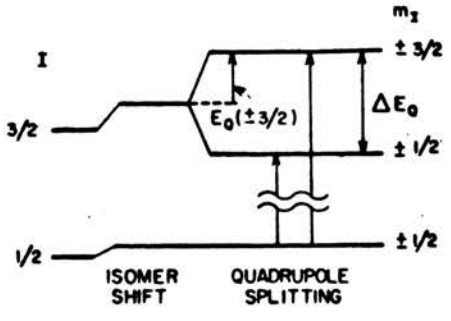

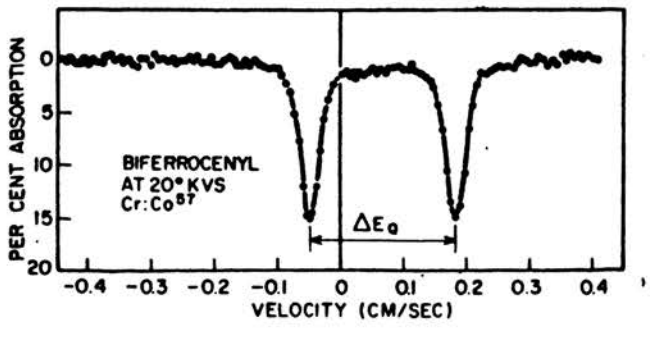

Figure 9. Quadrupole splitting in Fe^{57} (7, page 62).

and $m_I = I, I-1, \cdots, -I$ (7, page 72).

Thus a nuclear state of spin I will split into $2I+1$ energy levels. Transitions between the $I = \frac{3}{2}$ and $I = \frac{1}{2}$ spin states for Fe^{57} occur for $\Delta m_I = 0, \pm 1$ (see Figure 10). The relative intensities or per cent effects of the six absorption lines are 3,2,1,1,2,3 for an unpolarized absorber (9). The energy difference between any two equally intense lines in the magnetic hyperfine structure is proportional to the internal magnetic field. These splittings decrease as one increases the temperature until the Néel temperature, T_n, is reached. Above the Néel temperature, no magnetic hyperfine splitting occurs due to the lack of coupling of the atomic magnetic moments. Metallic iron has a Néel temperature of $T_n = 1043^{\circ}K$ and at room temperature has an internal magnetic field of 331 kilooersteds (20).

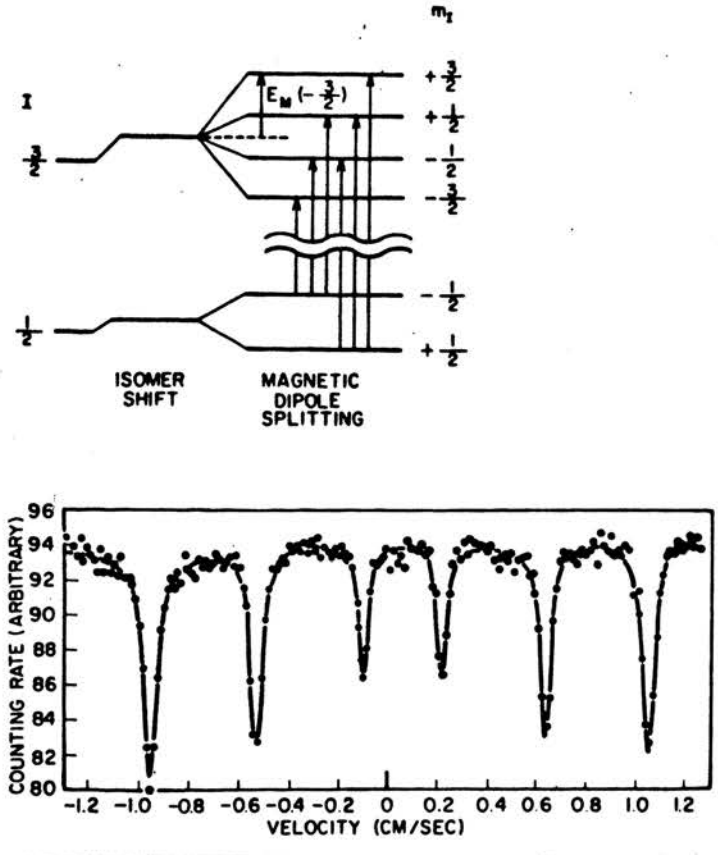

Figure 10. Magnetic hyperfine splitting of the ground and first excited state of Fe^{57} (7, page 73).

III. EXPERIMENTAL PROCEDURE

A. Velocity Drive Mechanisms.

Vibrational noise in any drive mechanism used for Fe^{57} Mössbauer studies must be very slight to prevent any distortion of the hyperfine spectrum. A drive mechanism which is electrically driven and is able to produce a voltage signal proportional to the source velocity provides a convenient check on the vibration and linearity of the system. For this reason, speaker type drive mechanisms were used. High compliance speakers proved to be more versatile than relatively stiff tweeter speakers. The first high compliance drive system used consisted of a speaker (University 8 inch, 30 watt) with its voice coil and cone mechanically connected to a linear velocity transducer (Sanborn 6LV2 LVsyn) as in Figure 11. Noise created by friction between the transducer magnet and its surrounding coil enclosure was found to be difficult to eliminate because of the limited adjustability of the transducer orientation with respect to the voice coil. As a result, a double speaker (two University 8 inch, 30 watt, Mössbauer speakers)system was built, using one speaker as a velocity drive mechanism and the other speaker as a velocity sensing mechanism (see Figure 12). The voice coils, although mechanically coupled, could be oriented independently of each other to insure free movement of each coil. The speaker cones and outer spiders were removed to decrease the restoring force on the voice coils and thus increase the compliance of the system. The frequency response for this system shows a resonant frequency of less than 10 cps and complex modes of oscillation do not

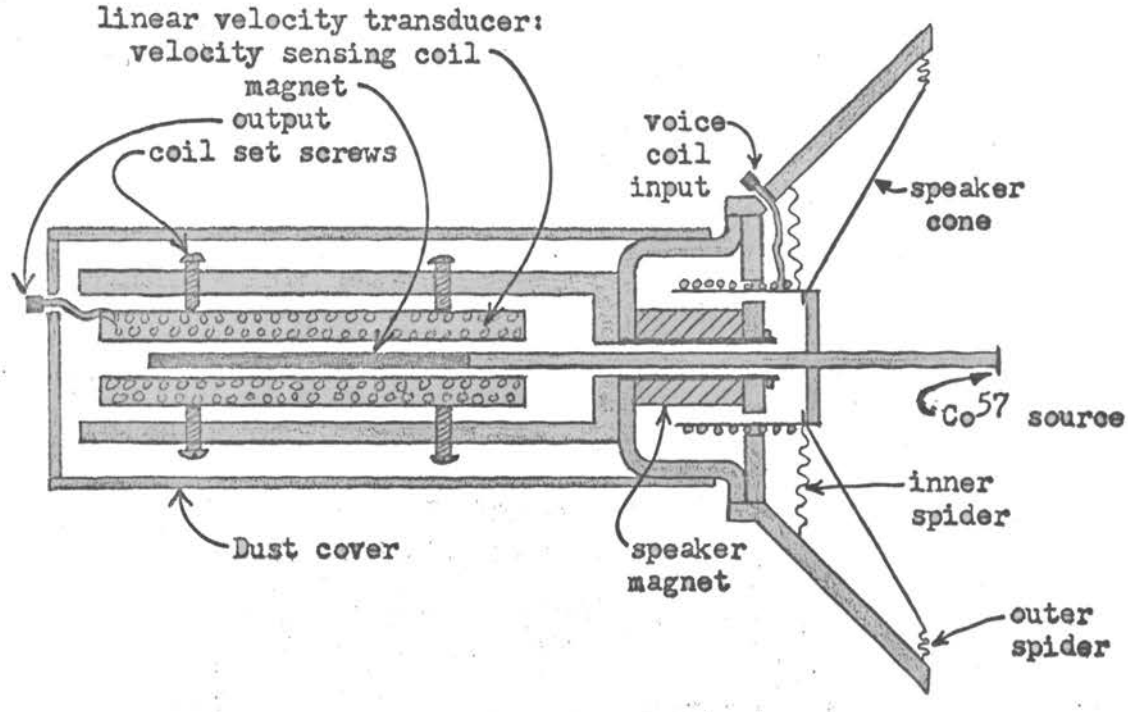

Figure 11. Speaker-transducer velocity drive system.

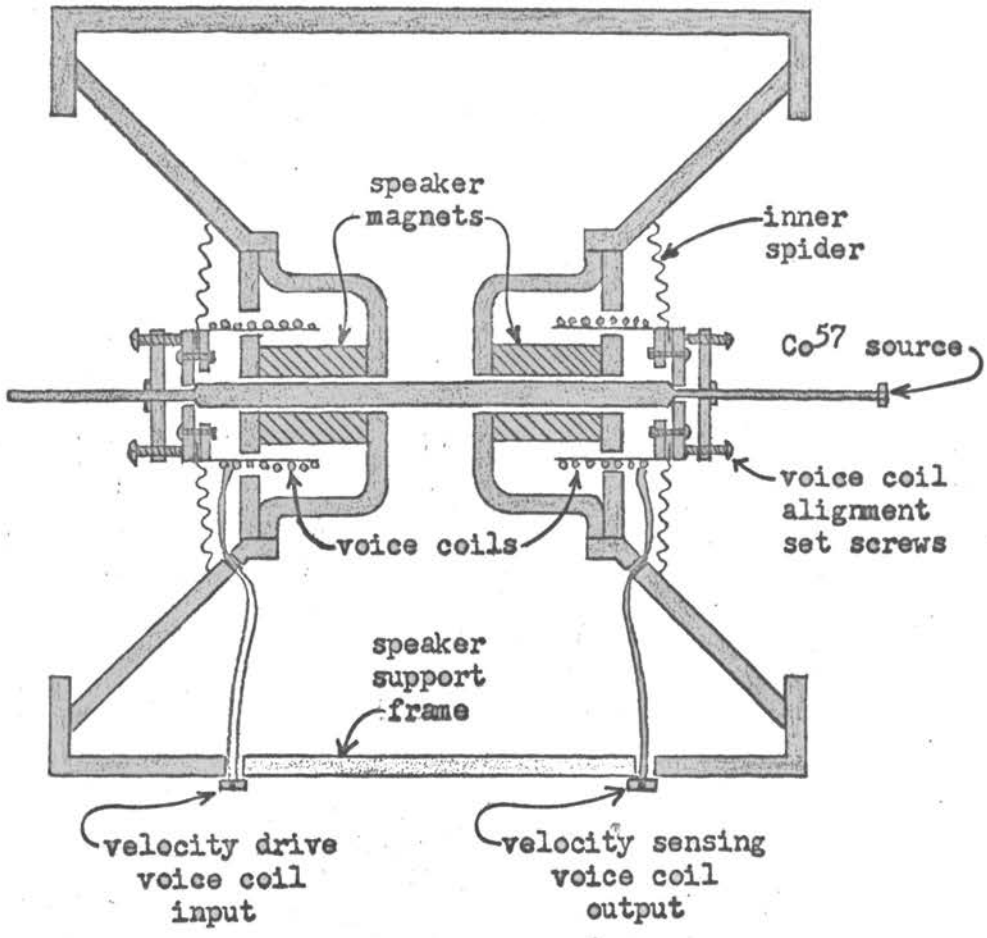

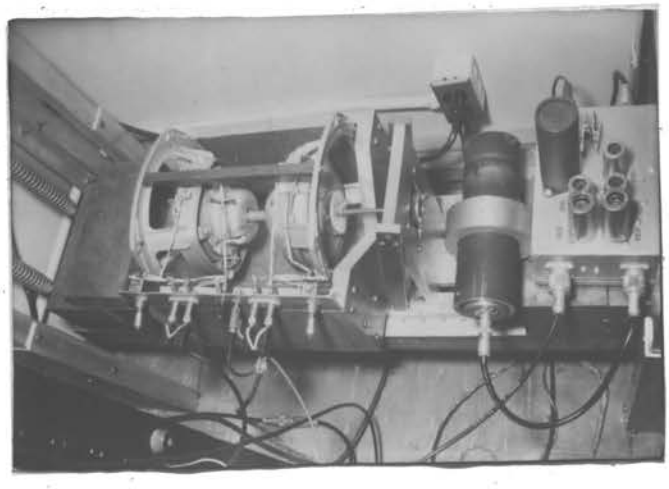

Figure 12. Double speaker velocity drive system.

develop until 2000 cps (see Figure 13). Excitation of unwanted modes of oscillation through vibration transmitted to the velocity drive system or to the absorber mounting framework was prevented by mounting both the velocity drive mechanism and absorber on a suspension system (see Figure 14). High frequency ringing in the four suspension springs was damped out by inserting foam rubber inside the spring coils. The period of oscillation for the 300 pound suspended Mössbauer bench was of the order of 1 second, and a velocity drive frequency of 25 cps was found to produce a vibration-free relative velocity between the source and the absorber. The velocity pick-up coil sensitivity was determined to be .0698 volts/cm/second for the double speaker velocity drive system.

B. Velocity Detection Modes.

1. Base line input.

The velocity signal from the pick-up coil must be used to obtain a gamma ray count rate versus velocity spectrum. The most convenient spectrum recording device is a multichannel analyser. Two modes of recording count rate versus velocity were investigated. The base line input mode consists of distributing gamma ray counts received at a pick-up coil velocity, V , to a channel number $C(v)$ where

$$C(v) = k_1 v + k_2$$

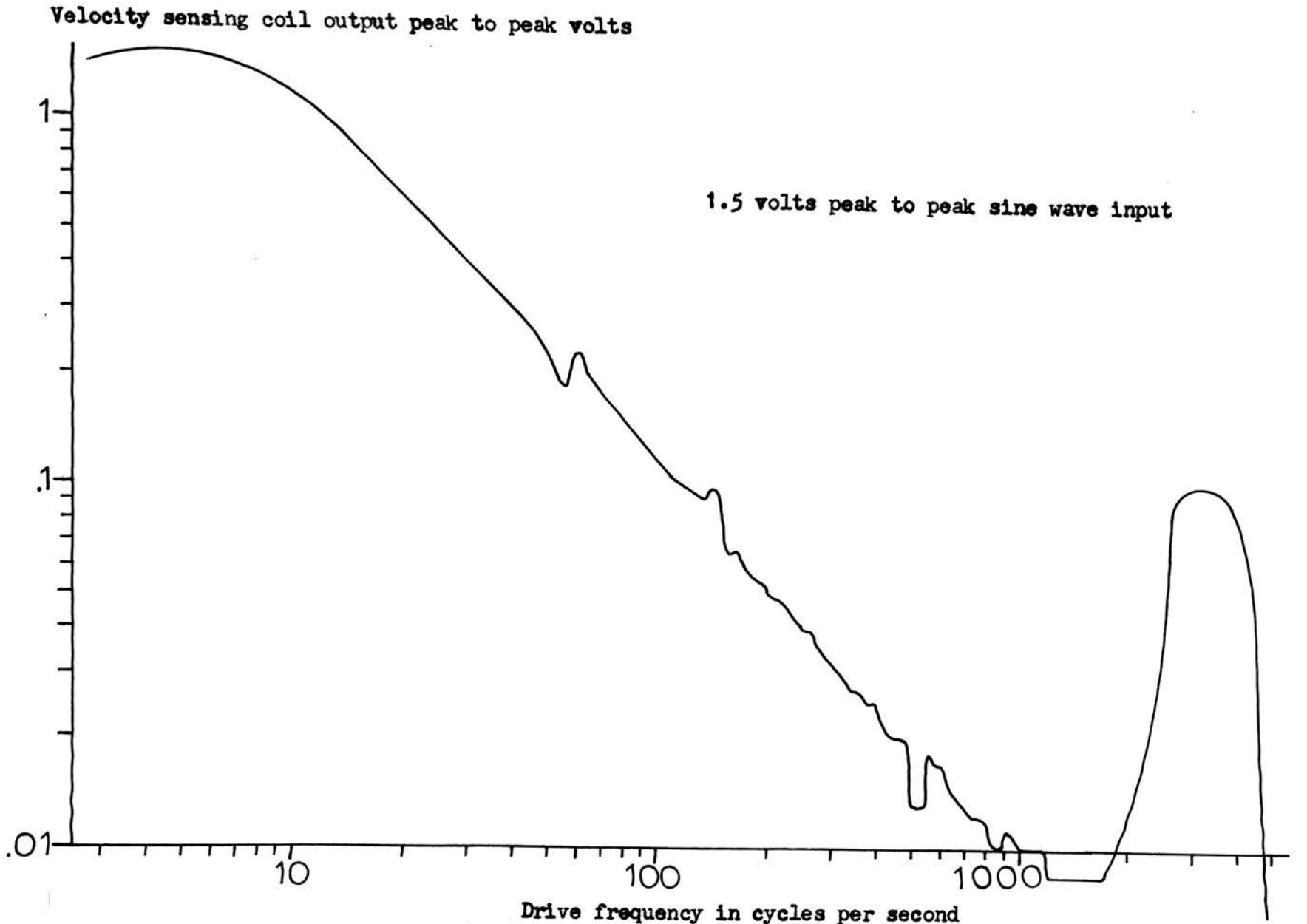

Figure 13. Frequency response for double speaker velocity drive system.

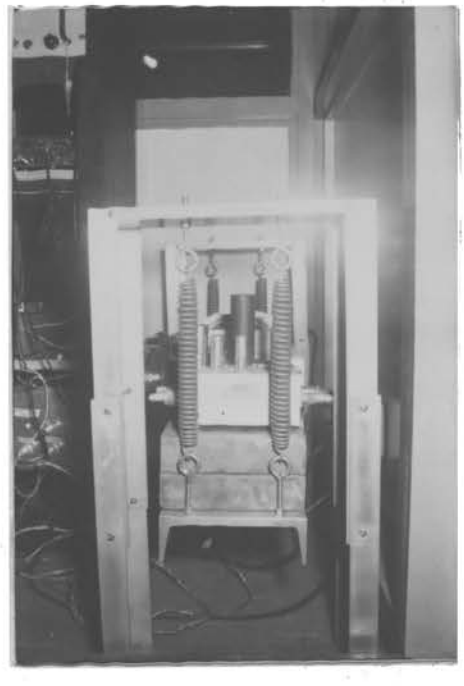

Figure 14. Suspension system for Mössbauer apparatus.

and k_1 = constant determining the number of channels per unit velocity.

k_2 = constant determining the relative position of the zero velocity channel.

This mode of operation produces a linear velocity scale but suffers from the disadvantage of not being able to discriminate between absorption lines and velocity nonlinearities. Thus if one can write

$$V = k_3 t + k_4$$

where k_3 = constant

k_4 = constant

t = time

then the Mössbauer spectrum will be flat (neglecting the absorption lines). If the velocity is not a linear function of time, the spectrum will have a non-flat shape in addition to any absorption lines. This arises because the amount of time spent near some velocity, V_1, is not equal to the amount of time spent near some other velocity, V_2, unless the velocity is a linear function of time. The spectrum for a sinusoidal velocity drive is a hyperfine absorption spectrum superimposed upon the $(\cos[2\pi f t])^{-1}$ probability distribution where f is the velocity drive frequency (see Figure 15).

2. Time base.

The time base mode consists of allowing each channel to receive counts for equal intervals of time. One period of oscillation of the velocity drive mechanism represents one

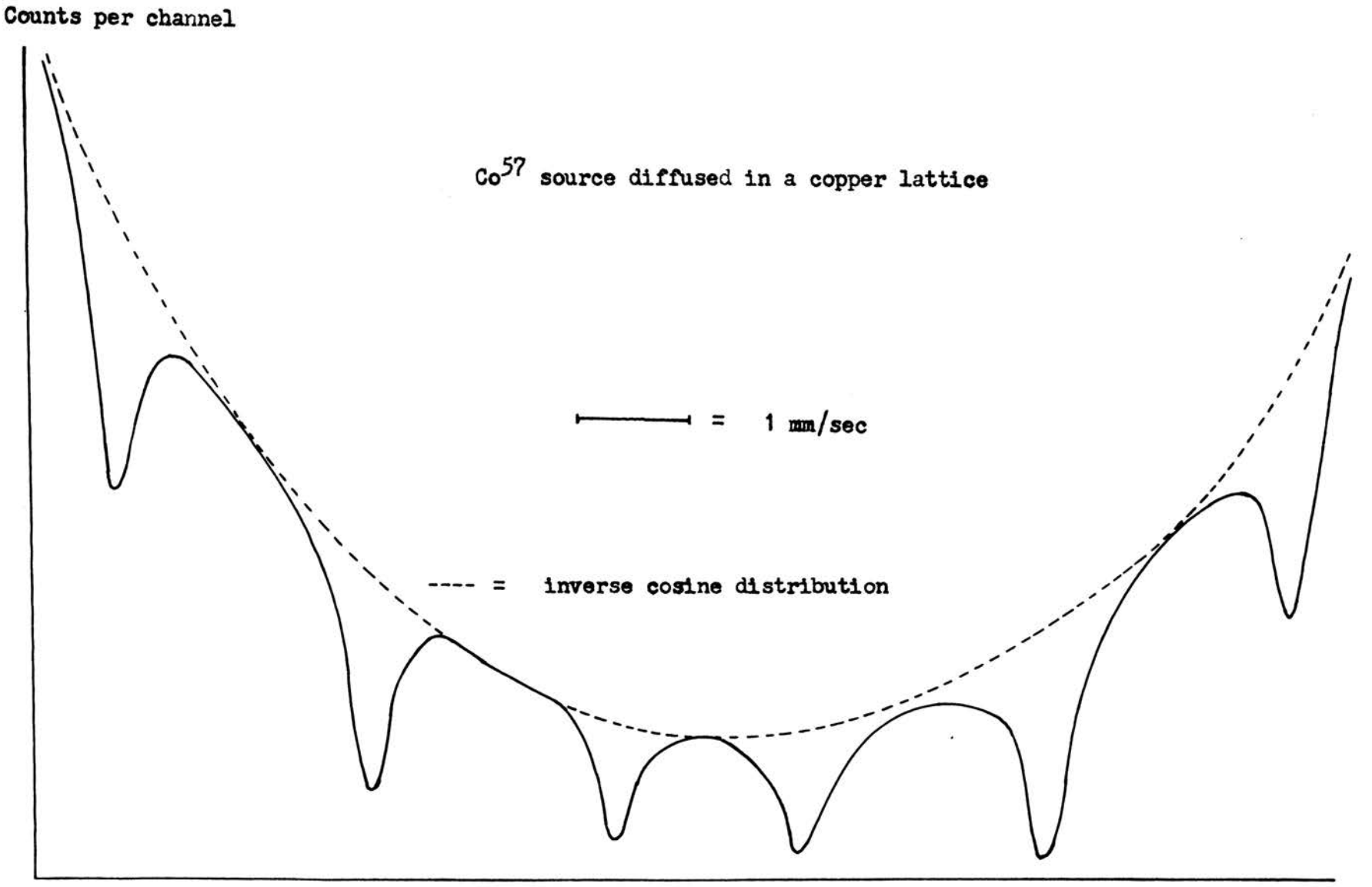

Figure 15. Natural iron hyperfine structure spectrum using sinusoidal velocity drive and baseline input mode.

sweep through all the channels of the multichannel analyser. This requires a synchronization of the multichannel analyser sweep frequency and the velocity drive frequency. The count rate versus velocity spectrum for this mode of detection produces a flat distribution if no absorption lines are present. Although the distribution is flat, independent of the wave shape of the velocity drive, the velocity scale will be linear only if the velocity is a linear function of time. For this reason, a triangular velocity wave shape was chosen for the time base detection mode.

C. Electronics.

The electrical drive signal necessary to produce a triangular velocity wave shape is the sum of a square wave acceleration term, triangular wave damping term, and a parabolic restoring force term (see Figure 16). One could electrically synthesize this drive signal, but a feedback network comparing the actual velocity signal with an ideal triangular reference velocity signal is a more convenient method of generating this desired velocity wave form. The block diagram of the electronics necessary for the time base detection mode using a triangular velocity wave shape is shown in Figure 17. The schematic diagram for the velocity reference signal electronics and feedback network is shown in Figure 18.

D. Source, Absorber, and Detector Geometry Considerations.

The per cent effect of the Mössbauer absorption lines is highly dependent upon the source, absorber, and detector geometry. This is particularly important if one wishes to detect small

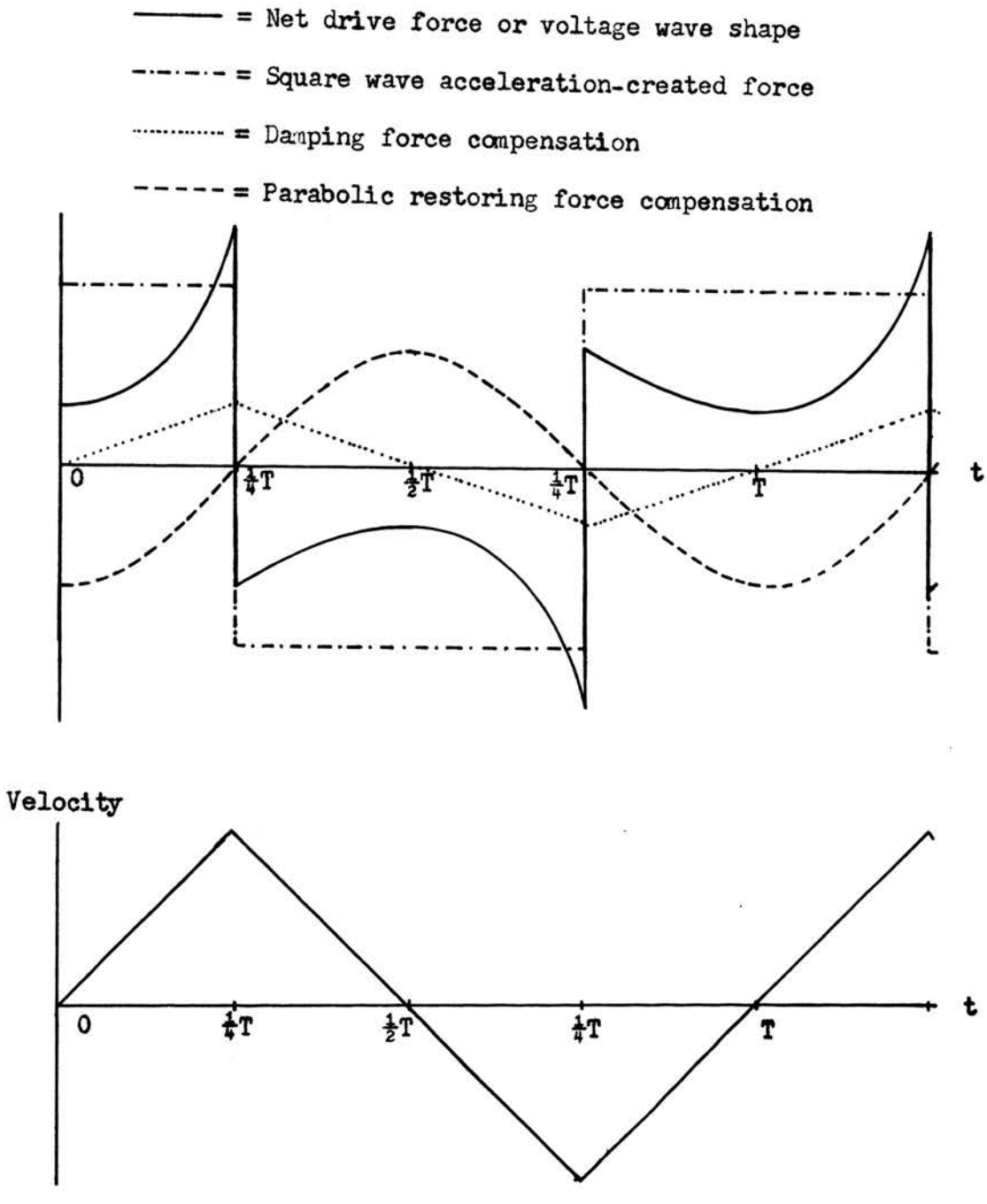

Figure 16. Triangular velocity drive signal.

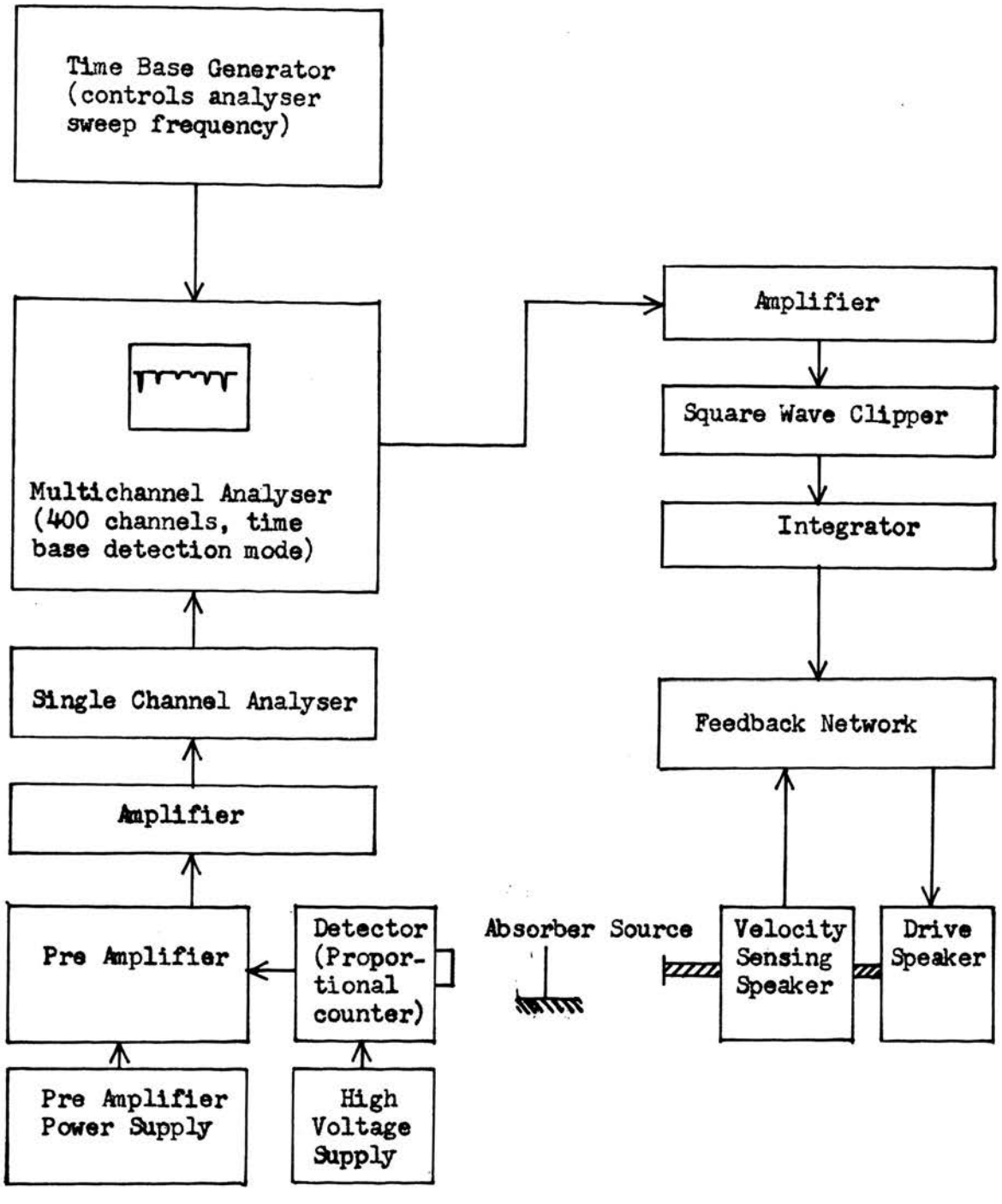

Figure 17. Block diagram for time base detection mode using a triangular wave velocity drive.

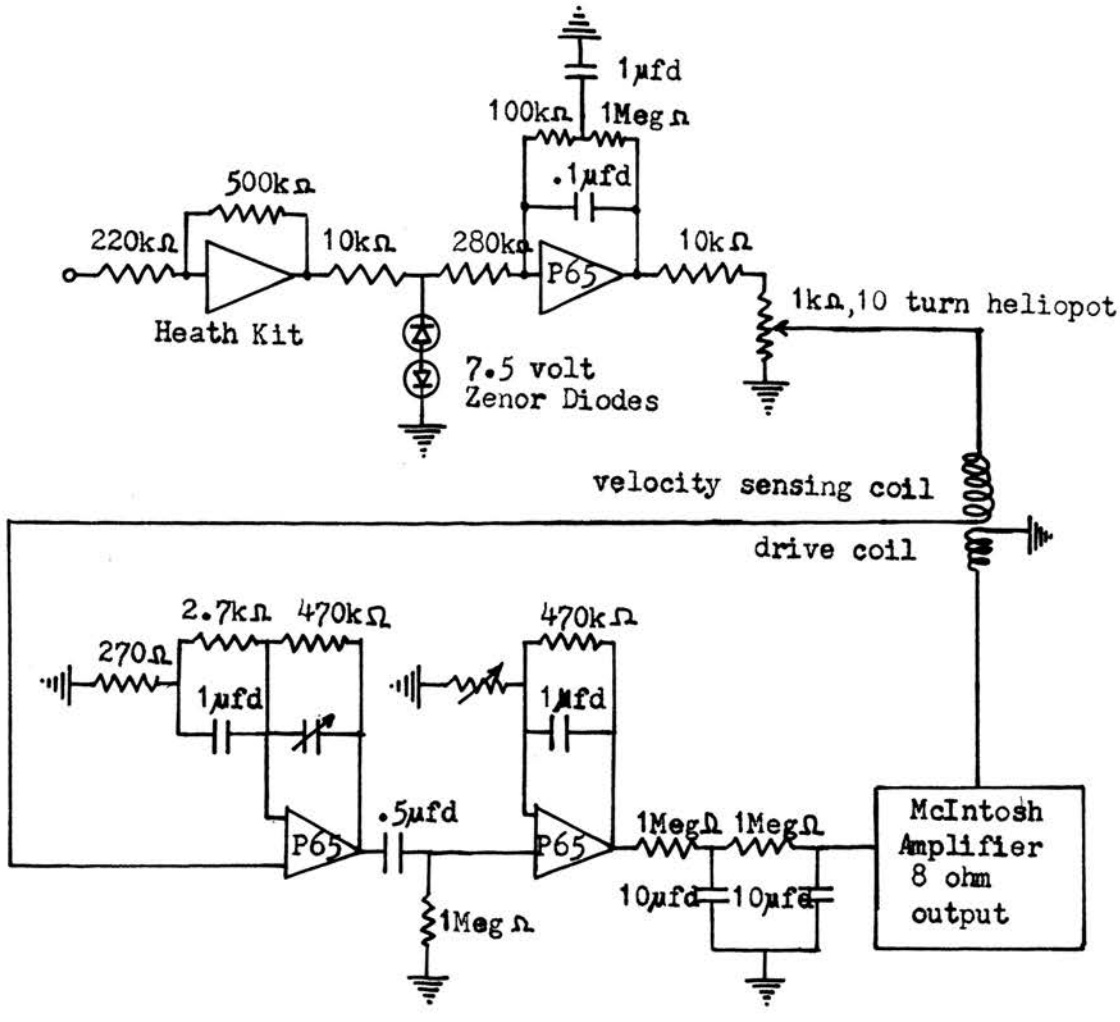

Figure 18. Schematic diagram for the reference signal electronics and feedback network.

absorption effects such as the hyperfine structure of Fe^{57} in $BiFeO_3$. For mathematical convenience, assume that the Co^{57} source is a point source isotropically emitting N, 14.37 kev gamma rays per second. The source is at a distance d from the round thin absorber of radius r and the absorber is at a distance D from the round detector window of radius R (see Figure 19). If the absorber is placed so that $D = 0$, then one sees only $\frac{1}{2}$ of the maximum decrease in count rate due to recoilless absorption. In this geometry, $\frac{1}{2}$ of the resonantly scattered gamma rays enter the detector window and are counted. Placing the absorber as far as possible from the detector window while changing r and d so as to keep

$$\frac{r}{d} = \tan^{-1}\theta = \text{constant} \quad ,$$

produces the highest fractional effect. This is true, since the mean solid angle the detector window subtends with the absorber is a minimum if $\frac{d}{D} << 1$. If one reduces θ, the per cent effect will also increase, but the gamma ray count rate will decrease because either the detector window is smaller or the source to detector distance is greater. One's ability to resolve or detect a Mössbauer absorption line depends upon fractional effect, F, per fractional standard deviation, S. The standard deviation for counting random nuclear gamma ray emissions (Poisson statistics) is simply the square root of the number of gamma ray counts (19, page 798). Using geometry considerations, one can derive

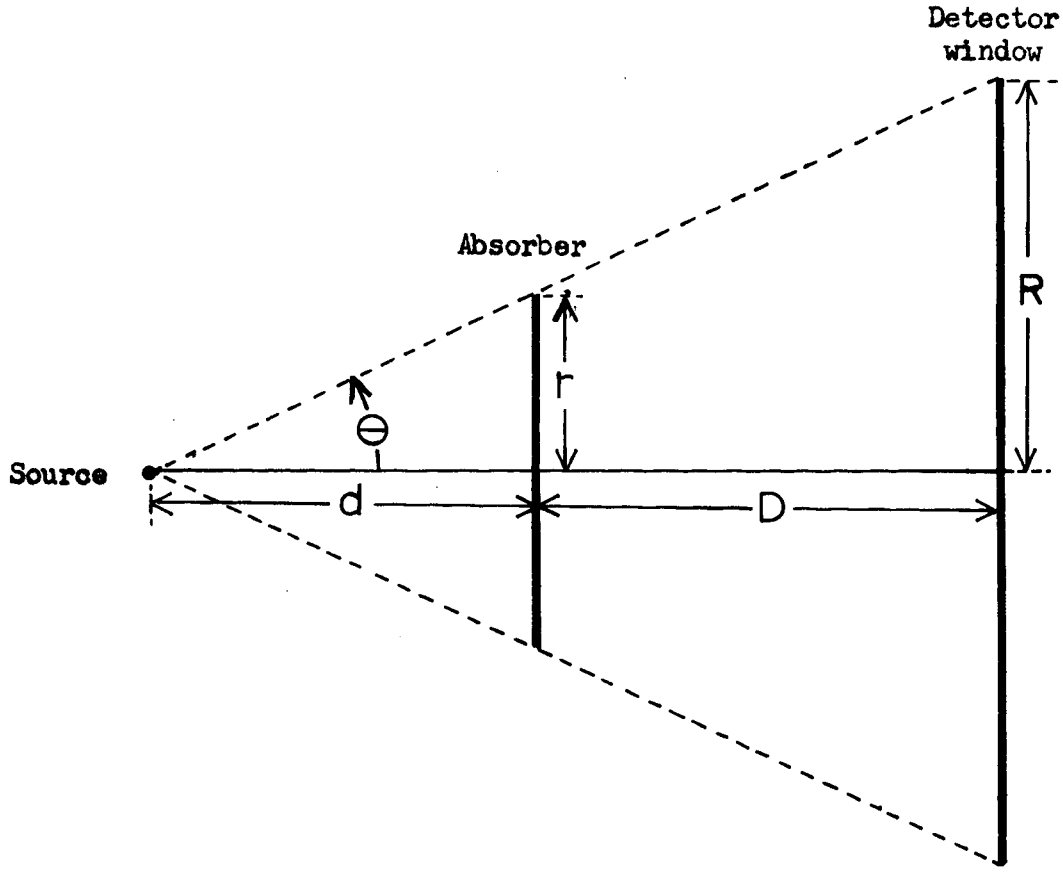

Figure 19. Source, absorber, and detector geometry.

$$\frac{F}{S} = \frac{\alpha}{8}\sqrt{\frac{N}{1-\beta}}\,(4\tan\theta - \tan^3\theta)$$

where α = fraction of incident 14.37 kev gamma rays that are resonantly absorbed and then isotropically emitted by the thin absorber.

β = fraction of incident 14.37 kev gamma rays nonresonantly absorbed by the thin absorber.

$$\frac{d}{D} << 1$$

Maximizing this equation with respect to θ yields

$$\theta = 49^\circ$$

for the largest fractional effect per fractional standard deviation. Using this large angle in an experiment would produce the undesirable result of linewidth broadening, because the gamma rays emitted by the source would be Doppler shifted by relative velocities ranging from

$$V \cos 0 = V$$

to

$$V \cos 49^\circ = .656\ V$$

As a result, an angle of $\theta = 10^\circ$ was used and found to produce a broadening 50 % smaller than the natural linewidth. The 2.54 cm diameter detector window thus required

$$D + d = 7.2 \text{ cm}$$

Mechanical limitations of the absorber support apparatus limited the ratio $\frac{d}{D}$ to

$$\frac{d}{D} = .33$$

where $d = 1.8$ cm

and $D = 5.4$ cm.

E. Absorber Thickness.

The absorber thickness (number of Fe^{57} nuclei per unit area) determines the probability of a gamma ray being resonantly scattered. If one uses a thick absorber, this Mössbauer scattering probability is high but the attenuation of the gamma rays by nonresonant absorption processes is also high. The absorber thickness dependence on the fractional effect per fractional standard deviation, $\frac{F}{S}$, can be understood if one adopts a mathematical model for the absorption process.

Let N_o = number per second of 14.37 kev gamma rays that are incident upon the absorber.

k = fraction of 14.37 kev gamma rays that are of the proper energy to be resonantly absorbed and scattered for the Mössbauer absorption line in question.

m_1 = mass per unit area of bakelite in the absorber disk (The $BiFeO_3$ was mixed with bakelite and then hot pressed to form a thin hard disk to be mounted on the absorber support device.).

m_2 = mass per unit area of $BiFeO_3$ in the absorber disk.

m_3 = mass per unit area of the Fe^{57} nuclei in the absorber because of the $BiFeO_3$ present.

μ_1 = absorption coefficient of bakelite in units of area per mass.

μ_2 = absorption coefficient of $BiFeO_3$ in units of area per mass (The small per cent effect of resonant absorption by the Fe^{57} nuclei can be neglected since the attenuation by the remaining 99.6% of the $BiFeO_3$ molecular weight is much greater than the attenuation caused by the Fe^{57} resonant absorption.).

μ_3 = absorption coefficient of Fe^{57} nuclei in units of area per mass of Fe^{57} nuclei (This absorption coefficient is the resonant absorption coefficient and is negligible if resonant absorption does not occur.).

Assuming an exponential count rate attenuation behavior in the absorber, the fractional effect is found to be

$$F = k\left(1 - e^{-\mu_3 m_3}\right)$$

as can be shown from Figure 20. The fractional standard deviation is

$$S = \frac{e^{\frac{1}{2}\sum_{i=1}^{2} \mu_i m_i}}{\sqrt{N_o}}$$

Thus the fractional effect per fractional standard deviation is

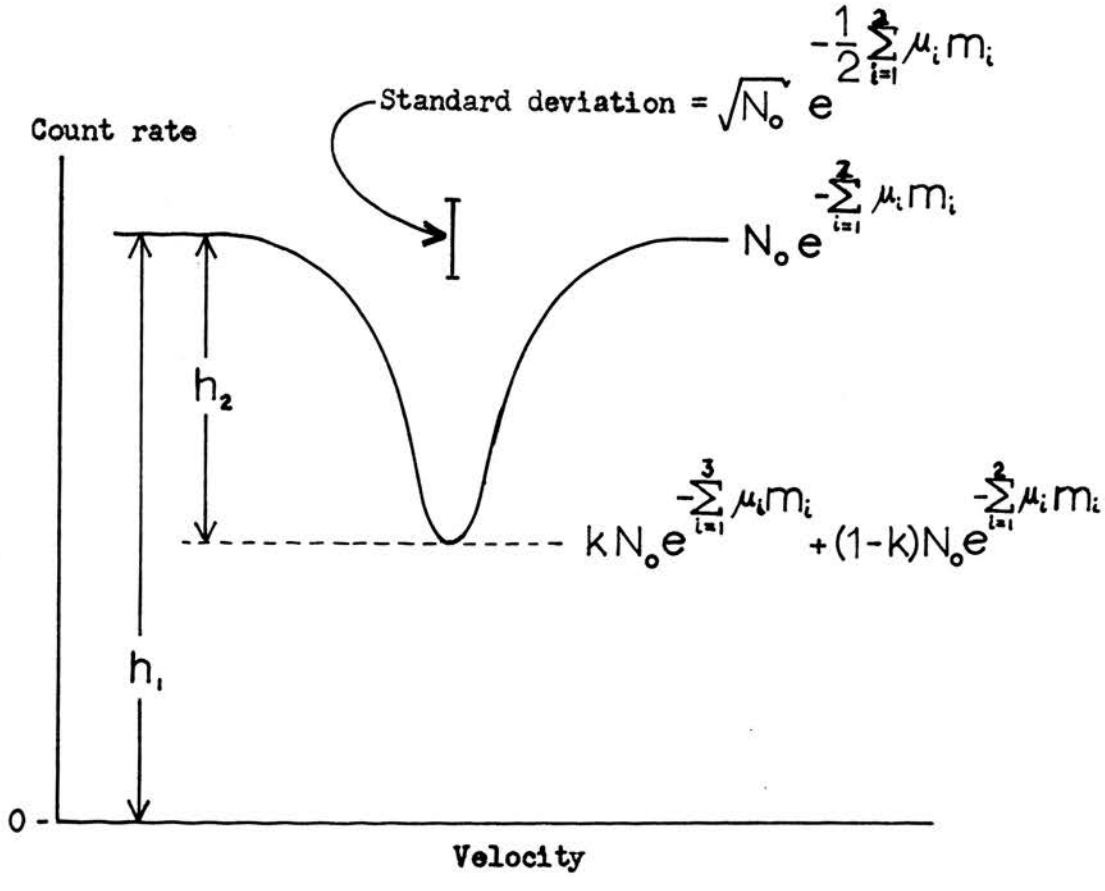

$$\text{Fractional effect} = F = \frac{h_2}{h_1} = k(1 - e^{-\mu_3 m_3})$$

Figure 20. Model Mössbauer spectrum.

$$\frac{F}{S} = k\sqrt{N_0}\left(1 - e^{-\mu_3 m_3}\right)e^{-\frac{1}{2}(\mu_1 m_1 + \mu_2 m_2)}$$

The mass of bakelite, m_1, is a constant for all the absorber samples used, but the mass of Fe^{57} nuclei m_3 is proportional to the mass of $BiFeO_3$, m_2. Thus

$$m_3 = \left(\frac{\text{atomic weight of } Fe^{57}}{\text{molecular weight of } BiFeO_3}\right)\left(\begin{matrix}\text{natural abundance}\\ \text{fraction of } Fe^{57}\end{matrix}\right)(m_2)$$

yielding $$m_3 = (.00409)(m_2)$$

and $$\frac{F}{S} = K_1\left(1 - e^{-\mu_3 K_2 m_2}\right)e^{-\frac{1}{2}\mu_2 m_2}$$

where $$K_1 = k\sqrt{N_0}\, e^{-\frac{1}{2}\mu_1 m_1}$$

$$K_2 = .00409$$

The maximum value of $\frac{F}{S}$ (see Figure 21) is found by setting

$$\frac{\partial\left(\frac{F}{S}\right)}{\partial m_2} = 0$$

m_2 = Mass per unit area of $BiFeO_3$ in absorber

F = Fractional effect

S = Fractional standard deviation = (Standard deviation)$^{-1}$

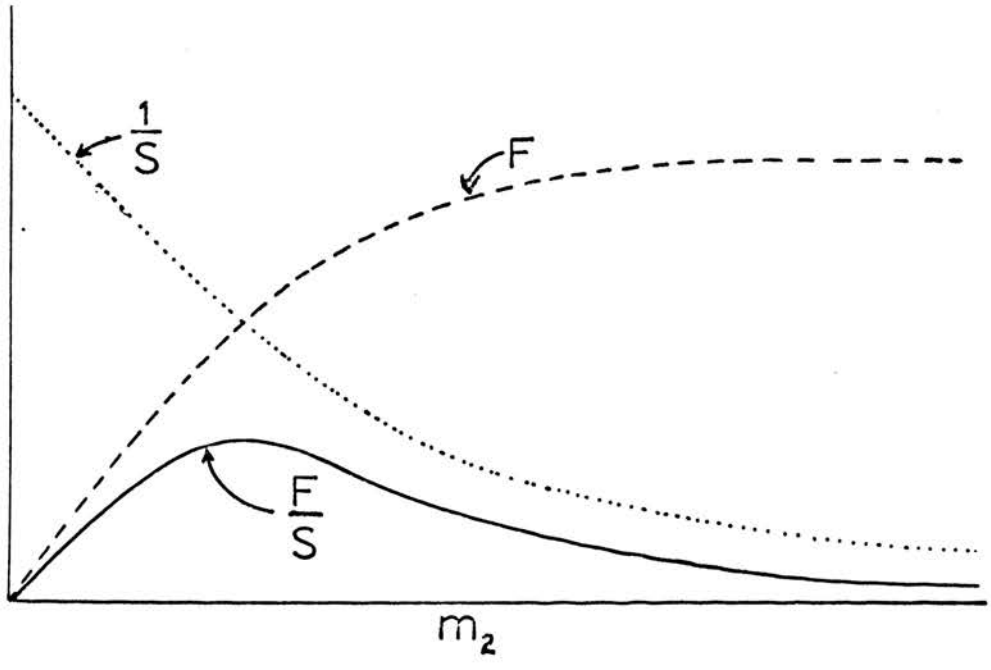

Figure 21. Fractional effect per fractional standard deviation versus absorber thickness.

where the optimum value of the mass of $BiFeO_3$ per unit area is

$$m_2 = \frac{1}{\mu_3 K_2} \ln \left(1 + \frac{2\mu_3 K_2}{\mu_2}\right) .$$

After the first $BiFeO_3$ Mössbauer spectrum was obtained, one could use the values for μ_2 and μ_3 to obtain a new value of m_2 and thus increase the fractional effect per fractional standard deviation. A value of $m_2 = 19.7$ mg/cm^2 was found to give the maximum $\frac{F}{S}$ value.

IV. DISCUSSION OF RESULTS

The hyperfine spectrum of $BiFeO_3$, shown in Figure 22, was obtained through the use of the time base detection mode, using a triangular velocity wave shape. The velocity calibration was computed by obtaining a Mössbauer spectrum for the known hyperfine structure lines of natural Fe without changing the velocity wave shape used for the $BiFeO_3$ spectrum. Thus the $BiFeO_3$ hyperfine spectrum is calibrated with respect to natural Fe. A 2 millicurie Co^{57} source diffused into a copper host lattice was used for the $BiFeO_3$ Mössbauer spectrum. The magnetic hyperfine splitting for the natural Fe calibration spectrum and that for the $BiFeO_3$ spectrum were compared to determine the internal magnetic field for $BiFeO_3$. Using this procedure, the internal magnetic field at the Fe lattice site in $BiFeO_3$, as determined from four different Mössbauer spectrums, was found to be (482 $\pm$ 9) kilooersteds. The additional central absorption peak is probably caused by a small amount of $Bi_2O_3 \cdot 2Fe_2O_3$ in a paramagnetic state. This impurity phase has a transition from the paramagnetic to the antiferromagnetic state at 265°K (21). It is difficult to remove and to detect (by x-ray diffraction) the small amounts of this paramagnetic impurity in the $BiFeO_3$. Quadrupole coupling in $BiFeO_3$ (at room temperature) is difficult to measure because of the experimental error in the velocity calibration. The natural Fe calibration spectrum is useful for velocities between -5.33 mm/sec and 5.33 mm/sec. One can only assume this calibration still applies for velocities above and below this range. Recent measurements taken above the

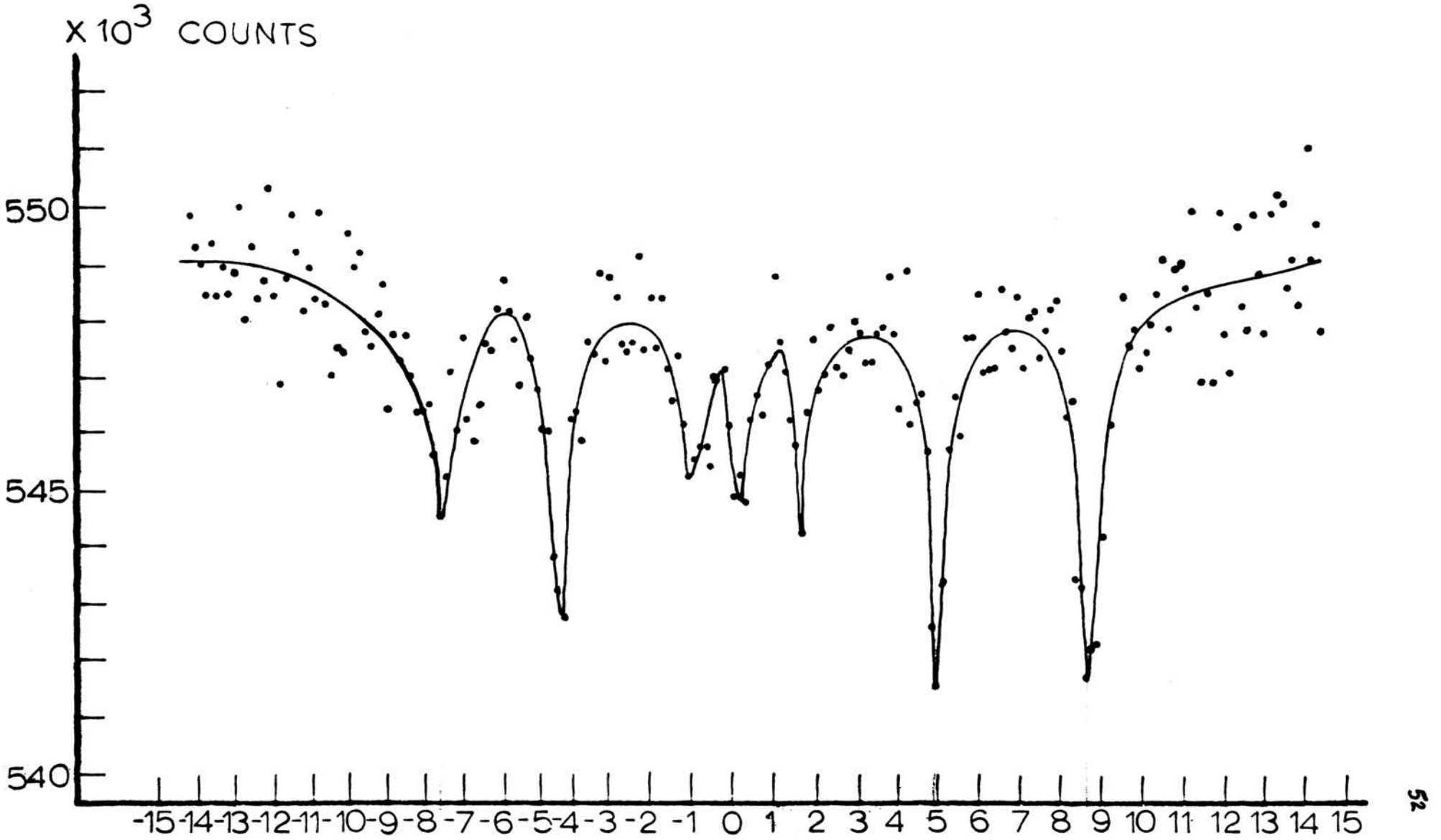

Figure 22. Hyperfine structure of $BiFeO_3$.

Néel temperature indicate strong quadrupole interaction in $BiFeO_3$ (22). The Debye temperature for $BiFeO_3$ can be computed if one assumes the Young's modulus to be approximately the same as for other ceramics of similar structure. Using this method, one obtains $\Theta_D \cong 220^\circ K$. The recoilless fraction f can also be determined if one assumes $\Theta_D \cong 220^\circ K$. As a result, (see Figure 23) one obtains $f = .48$. One could increase f by resorting to a low temperature absorber.

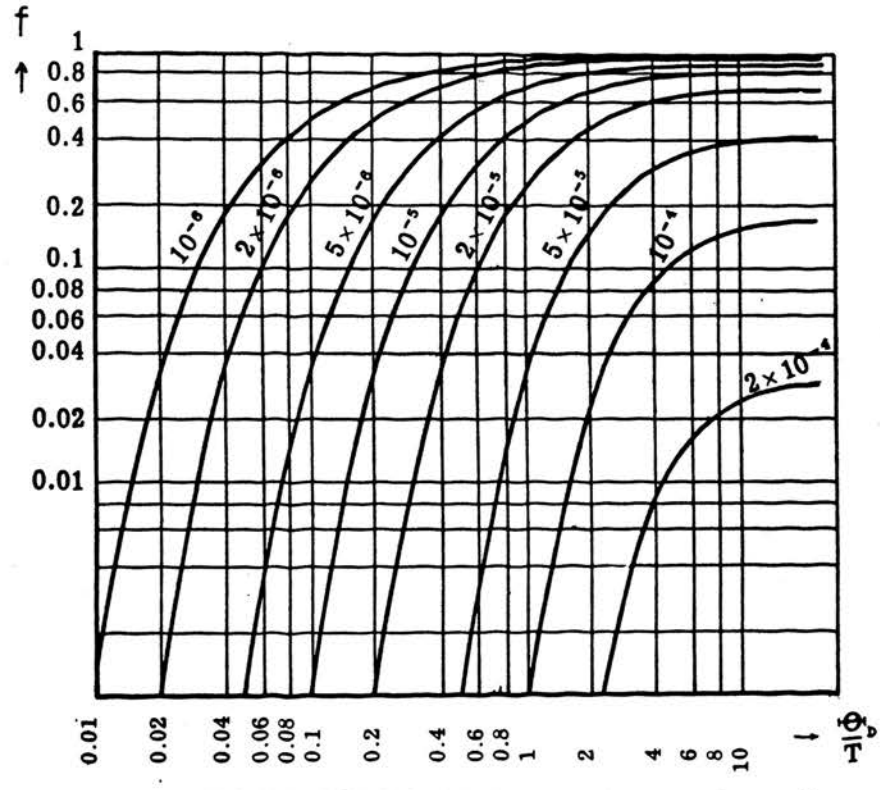

The parameter labeling each curve is $\frac{E_R}{\Theta_D}$

For $BiFeO_3$:

$\frac{E_R}{\Theta_D} = 8.7 \times 10^{-6}$ ev/°K

$\frac{\Theta_D}{T} = .74$

Figure 23. Recoilless fraction as a function of $\frac{E_R}{\Theta_D}$ and $\frac{\Theta_D}{T}$, (4, page 48).

V. CONCLUSIONS

The magnetic hyperfine structure of the Fe^{57} nucleus in the antiferromagnetic $BiFeO_3$ lattice was investigated by the Mössbauer effect. Hyperfine structure measurements yielded an internal magnetic field of (482 ± 9) kilooersteds at the Fe^{57} nuclei at room temperature. No experimentally observable quadrupole coupling was found to exist.

BIBLIOGRAPHY

1. HODGMAN, C.D. (1958-1959) Handbook of chemistry and physics. 40th ed., Chemical Rubber Publishing Co., Cleveland, p. 456.

2. CHOU, PEN-CHU, (1966) An x-ray study of the lead zirconate - bismuth ferrate system. Thesis, The University of Missouri at Rolla, Missouri. 101 p (with 49 figures, 7 tables.)

3. SMOLENSKII, G.A., V.M. YUDIN, E.S. SHER, and YU.E. STOLYPIN (1963) Antiferromagnetic properties of some perovskites. Soviet Physics JETP, vol. 16, no. 3, p. 622-624.

4. FRAUENFELDER, HANS (1963) The Mössbauer effect. W.A. Benjamin, New York. 336 p.

5. WOOD, R.W., (1954) Physical optics. New York, Macmillan.

6. MÖSSBAUER, R.L., (1958) Kernresonanzfluoreszinz von gammastrahlung in Ir^{191} (Nuclear resonance absorption of gamma rays in Ir^{191}). Z. Physik, 151, p. 124.

7. WERTHEIM, GUNTHER K., (1964) Mössbauer effect: principles and applications. Academic Press, New York. 116 p.

8. LIPKIN, HARRY J., (1960) Some simple features of the Mössbauer effect. Annals of Physics 9, p. 332-339.

9. HANNA, S.S. and R.S. PRESTON (1965) Mössbauer cross section of Fe^{57} in iron. Physical Review vol. 139, no. 3A, p. A722-A725.

10. MARGULIES, S. (1962) The Mössbauer effect in iron - 57, Thesis, The University of Illinois.

11. MAIER, H. and LEIBNITZ (1961) Inverted pendulum velocity drive. Proceedings of the Second International Conference on the Mössbauer effect held at Saclay, France on September 13-15, 1961. John Wiley and Sons, Inc., New York. 314 p.

12. MÖSSBAUER, R.L., (1961) Constant cam velocity drive. Proceedings of the Second International Conference on the Mössbauer effect held at Saclay, France on September 13-15, 1961. John Wiley and Sons, Inc., New York. 314 p.

13. LYNCH, F.J., and J. B. BAUMGARDNER (1961) Transducer for Mössbauer experiments. Proceedings of the Second International Conference on the Mossbauer effect held at Saclay, France on September 13-15, 1961. John Wiley and Sons, Inc., New York. 314 p.

14. PERLOW, G. J. (1961) Automatic lead screw constant velocity drive. Proceedings of the Second International Conference on the Mössbauer effect held at Saclay, France on September 13-15, 1961. John Wiley and Sons, Inc., New York. 314 p.

15. BOYLE, A.J.F. (1961) Experimental determination of lattice properties. Proceedings of the Second International Conference on the Mössbauer effect held at Saclay, France on September 13-15, 1961. John Wiley and Sons, Inc., New York. 314 p.

16. POUND, R.V. and G.A. REBKA (1960) Apparent weight of photons. Physical Review Letters, vol. 4, no. 7, p. 337-341.

17. BOMMEL, H.E. (1961) Measurement of the frequency shift of gamma rays using the Mössbauer effect. Proceedings of the Second International Conference on the Mössbauer effect held at Saclay, France on September 13-15, 1961. John Wiley and Sons, Inc., New York. 314 p.

18. GRADZINS, L. and E.A. PHILLIPS (1961) Phase modulation of gamma rays. Proceedings of the Second International Conference on the Mössbauer effect held at Saclay, France on September 13-15, 1961. John Wiley and Sons, Inc., New York. 314 p.

19. EVANS, ROBLEY D. (1955) The atomic nucleus. New York, McGraw-Hill, 972 p.

20. HANNA, S.S., R.S. PRESTON, and J. HEBERLE (1961) Temperature dependence of the Mössbauer effect in metallic Fe^{57}. Proceedings of the Second International Conference on the Mössbauer effect held at Saclay, France on September 13-15, 1961. John Wiley and Sons, Inc., New York. 314 p.

21. TUTOV, A.G., I.E. MYL'NIKOVA, N.N. PARFENOVA, V.A. BOKOV, and S.A. KIZHAEV (1964) New compounds in the systems Bi_2O_3-Me_2O_3 (Fe^{3+}, Al^{3+}, Ga^{3+}, Mn^{3+}). Soviet Physics - Solid State, vol. 6, no. 3, p. 963-964.

22. BHIDE, V.G. and M.S. MULTANI (1965) Mössbauer effect in ferroelectric-antiferromagnetic $BiFeO_3$. Solid State Commun. (U.S.A.), Vol. 3, no. 9, p. 271-4.

VITA

The author was born March 12, 1942, in Cleveland, Ohio. He received his primary and secondary education in Rocky River, Ohio. He has received a Bachelor of Science Degree in Physics from Case Institute of Technology, in Cleveland, Ohio. The author has been enrolled in the Graduate School of the University of Missouri at Rolla since September, 1964, and has been a research fellow during this period of time.

The author is married to the former Judith Sturgeon.